communications earth & environment

Article

A Nature Portfolio journal

https://doi.org/10.1038/s43247-026-04120-8

Persistent seasonal deoxygenation alters benthic metabolic processes and accelerates hypoxia feedbacks in the Baltic Sea

Check for updates

Shuba Varshini Alampalli[1,11], Stefanie Böhnke-Brandt[2,11], Nicole Adam-Beyer[2], Katja Laufer-Meiser[2], Klaus Wallmann[3], Hermann W. Bange[4], Helmke Hepach[5], Matthias Thiele[2], Florian Scholz[6], Emanuel Wyler[7], Markus Landthaler[7,8], Isabel Diercks[9], Janina Fuß[10] & Mirjam Perner[2] ✉

Nutrient enrichment and warming cause widespread costal deoxygenation, leading to hypoxia or even anoxia in bottom waters. The benthic-water-column-feedbacks that develop under persistent seasonal oxygen depletion and amplify hypoxia remain poorly constrained. A 15-month study of a seasonally hypoxic to anoxic costal system in the southwestern Baltic Sea combined water-column monitoring, sediment chemistry, metabolic rates and microbial analyses with historic data to reveal pronounced seasonal shifts in sediment processes. During winter oxygenation, organic matter degradation, fermentation, aerobic respiration, nitrate- and iron-reduction and microbial competition increased. Re-ventilation following anoxia did not reset sediment biogeochemistry, but initiated intensified oxygen consumption, microbial biosynthetic activity and anaerobic carbon re-cycling. Reactive ironoxyhydroxides became exhausted, the sulfidic zone shoaled and sulfate reduction and pyrite formation rates increased through fall. These processes reinforced benthic feedbacks, progressively reducing the sediment's capacity to retain sulfide over years. This weakening of sedimentary resilience exacerbates sulfide accumulation in eutrophic costal environments with growing chances of sulfidic deep-water upwelling.

In the last 50 years, oxygen (O_2)-depleted waters have expanded rapidly in the open oceans and coastal regions, with fundamental consequences for marine biodiversity, biological productivity and biogeochemical cycling[1–4]. In the Baltic Sea, the spread of hypoxia ($O_2 < 63$ µM) is driven both by climate change and eutrophication[4,5]. Ecosystem response to these stressors occurs at considerably higher rates in the Baltic Sea than in the global ocean[6–8], making it a natural laboratory for assessing and forecasting the combined effects of regional and global anthropogenic pressures[9].

The long-term time-series station Boknis Eck, in the south-western Baltic Sea, exemplifies these dynamics. Located in shallow waters (28 m), the site is exposed to seasonal water column stratification and deoxygenation. Algal blooms occurring in late winter and summer fuel particulate organic carbon (POC) fluxes to the seabed[10], resulting in organic-rich sediments (~5 wt.% C_{org})[11,12]. Microbial remineralization of this labile organic matter (OM) drives benthic O_2 consumption[13]. During winter, the water column is well mixed resulting in oxygenated bottom waters. In spring, density-stratified waters start developing as colder, saline water from the North Sea

[1]Core Unit Bioinformatics, Berlin Institute of Health at Charité-Universitätsmedizin, Berlin, Germany. [2]Geomicrobiology, GEOMAR Helmholtz Centre for Ocean Research Kiel, Kiel, Germany. [3]Benthic Biogeochemistry, GEOMAR Helmholtz Centre for Ocean Research Kiel, Kiel, Germany. [4]Chemical Oceanography, GEOMAR Helmholtz Centre for Ocean Research Kiel, Kiel, Germany. [5]Biological Oceanography, GEOMAR Helmholtz Centre for Ocean Research Kiel, Kiel, Germany. [6]Department of Earth System Sciences, University Hamburg, Hamburg, Germany. [7]Max-Delbrück-Center for Molecular Medicine in the Helmholtz Association (MDC), Berlin Institute for Medical Systems Biology (BIMSB), Berlin, Germany. [8]Institut für Biologie, Humboldt-Universität zu Berlin, Berlin, Germany. [9]Marine Mineral Resources, GEOMAR Helmholtz Centre for Ocean Research Kiel, Kiel, Germany. [10]Competence Centre for Genomic Analysis (CCGA), Institute of Clinical Molecular Biology (IKMB), Kiel University, Kiel, Germany. [11]These authors contributed equally: Shuba Varshini Alampalli, Stefanie Böhnke-Brandt. ✉e-mail: mperner@geomar.de

underlies warmer, less saline waters[13]. This progressively restricts ventilation and enhances bottom water O_2-depletion[14]. By late summer, deep waters can become anoxic and even sulfidic[15,16]. In fall, cooling and storm-driven mixing break stratification and re-establish oxygenated deep-waters[13]. Although external nutrient loads to the Baltic Sea have been reduced in the last decades[17], hypoxic events at Boknis Eck have increased in frequency, consistent with intensified warming, stratification and bacterial biomass production[10,15]. This was accompanied by an upward shift of the sulfide zone towards the sediment surface[18].

Seasonal hypoxia in coastal systems exerts strong pressures on benthic microbial communities, triggering shifts from aerobic to anaerobic metabolisms[18–21]. This considerably alters sedimentary biogeochemical cycles[22,23], favoring sulfate reduction (SR) and accumulation of reduced compounds[18,24,25], while increasing nutrient fluxes across the sediment-water interface[12,26]. Besides O_2 availability, benthic OM degradation and Fe-S-cycling substantially affect sediment redox chemistry and Fe/S-bistability[27]. Importantly, seasonal hypoxia not only alters microbial metabolisms but also suppresses bioturbation and bioirrigation, weakening sediment ventilation, reducing recycling of reactive Fe minerals and promoting a shift toward persistent sulfidic sediment conditions[28,29]. The interplay between Fe(III)-reduction, sulfide production and Fe-S-mineral formation thereby governs whether an Fe-rich-low-sulfide (ferruginous) or a sulfide-rich-low-Fe (sulfidic) state exists[27]. Such benthic mechanisms can contribute to prolonged O_2 deficiency in stratified coastal waters. Yet, underlying mechanisms for bidirectional feedbacks between seasonal water O_2 dynamics and benthic microbial functioning and biogeochemistry over annual time scales are still poorly constrained. We hypothesize that persistent seasonal deoxygenation shifts benthic microbial communities toward sustained anaerobic metabolisms and depletes reactive Fe-mineral reservoirs. This would progressively reduce the sediment's capacity to buffer hydrogen sulfide and accelerate self-reinforcing feedbacks that reduce long-term sedimentary resilience.

We investigated benthic feedbacks to seasonal hypoxia at Boknis Eck via a 15-month observational study, integrating sediment biogeochemistry, microbial activity and water column variations. We quantified in situ O_2 consumption rates at the sediment-water interface and followed changes in sediment properties using sequential Fe extractions, porewater chemistry, measured and modeled metabolic rates and microbial cell counts. Changes in benthic microbial communities were studied via 16S amplicon sequencing for most of the 15 months, whereas metagenomic and metatranscriptomic analyses focused on surface sediments collected in winter, when bottom waters were oxygenated, and in fall, following re-ventilation of bottom waters after a phase of summer anoxia. Together, these data provide a mechanistic framework for understanding and predicting how seasonal deep-water O_2 depletion restructures benthic processes.

Results

Seasonal water column dynamics and benthic fluxes

Water column properties between January 2022 and March 2023 followed a common seasonal cycle at Boknis Eck[10,15] (Figs. 1 and S5): From January to March, the water body was well ventilated with little vertical differences in temperature and O_2 concentrations (Fig. 1A, B). Stratification started developing in April, intensifying during summer with rising surface water temperatures and progressively O_2-depleted bottom waters reaching anoxia in September. In October, water column stratification broke, as indicated by converging surface and bottom water temperatures, re-establishing oxygenated conditions at the seafloor (Fig. 1A, B). Deep-water nitrate (NO_3^-) and nitrite (NO_2^-) concentrations were highest during periods of well-ventilated bottom waters in February/March but lowest during summer stratification (cf. Fig. 1A, C). By contrast, benthic phosphate (PO_4^{3-}) release reached a maximum during September anoxia (Fig. 1C)[12]. Dissolved Fe and Mn concentrations in benthic chamber waters were elevated in late August and decreased again during October (Figs. 1D and S6). O_2 consumption in early October enclosed chamber experiments re-installed anoxic deep waters and induced benthic Fe and Mn release again (Figs. 1D, S6 and S7). While dissolved Fe and Mn concentrations in porewaters of surface near sediments progressively increased during late winter, in late October, only dissolved Mn was high near the sediment surface, but dissolved Fe remained undetected (Fig. S7). Water column Chl a levels indicated phytoplankton blooms and primarily POC export to the seafloor in February 2022 (no data for March), July 2022 and March 2023 (Figs. 1E and S5), consistent with previous years[15]. Methane was measured for March to May and August to October 2022 in water samples: Highest methane concentrations at 25 m were measured in April (360 nM CH_4) and September (343 nM CH_4) 2022 (Fig. 1E) following periods of high surface productivity. Benthic O_2 consumption rates determined in benthic chambers were highest in March and early October 2022 (Figs. 1F and S7).

Sediment redox processes and seasonal biogeochemical cycling

Measured SRR exhibited strong seasonality with highest rates between August and late October and maxima at the sediment surface (Figs. 1F and S8). In comparison, peak SRR in winter was tenfold lower and deeper (1–2 cm). Porewater profiles mirrored this trend with both highest and shallowest dissolved sulfide accumulations occurring between August and October (Fig. S8), aligning with previous observations[12,18,24,25]. Reactive transport models predicted the highest rates for S_{ox} and sedimentary pyrite (FeS_2) formation in late October and for $POC_{ox\text{-}subox}$ degradation (via aerobic respiration, NO_3^-, Mn(IV) and Fe(III) reduction) in early October (Fig. 2A–C). Alkalinity and NH_4^+ were considerably elevated in late October near the sediment surface (Fig. S8). In sequential Fe-extractions, Fe(II) was the predominant redox species across all months, contributing to the majority of the Fe extracted from sediments (Fig. 3). The only exception was February, where Fe(III) contributed up to >50% in 0–1 cm sediments. Although absolute Fe(III) abundances may be slightly overestimated because of unavoidable sample handling (see "Methods"), the February samples remained distinct from all other months. Fe(II) concentrations in amorphous minerals (e.g., FeS and Fe-carbonates) were highest in late October surface sediments, whereas Fe(II) concentrations in crystalline minerals (including Fe(II)-silicates, magnetite and to some extent FeS_2) peaked in August and early October.

Cell numbers and composition of sedimentary microbial consortia

Cell numbers of surface sediments were highest between March and early October 2022 and dropped 50% by the end of October, remaining high at around 2×10^9 cells mL^{-1} sediment until March 2023 (Figs. 1G and S9) - in line with previous observations[18]. Taxonomic assignments via 16S rRNA gene amplicons revealed microbial succession over time and a distinct vertical distribution (Figs. 2D and S10A–C). Shifts in taxa were evident for the different seasons: The January 2022 top sediments contained putative sulfur-oxidizing bacteria (SOB) (70%), declining in February (38%) and March (26%) and reaching a peak low in May (7%). SOB increased again from July to early October (~20%), reaching higher levels in late October 2022 and January 2023 (33%), before declining again by March 2023 (15%). More differences in SOB between winter 2022 and 2023 are detailed in Text S6. In contrast to SOBs, the proportion of OM degraders increased from 6% in January to 43% in May 2022, mainly driven by *Pirellulaceae* (*Planctomycetota*, 23%) and the Pla4 lineage (8%). From May to late October, SRB kept increasing (from 6% to 16%). Other organotrophs decreased until early October 2022, remaining around 17% until March 2023. Conversely to Bacteria, the archaeal consortium stayed remarkably stable during the 15 months, with members of *Bathyarchaeia*, *Lokiarchaeia*, Marine-Benthic-Group D/DHVEG-1, *Woesearchaeales* and *Nitrosopumilaceae* constituting the core taxa (Fig. S10C).

Metabolic potential revealed by metatranscriptome data

Analyses of metagenome and metatranscriptome data from February, March, early October and late October 2022 yielded 99 Metagenome-

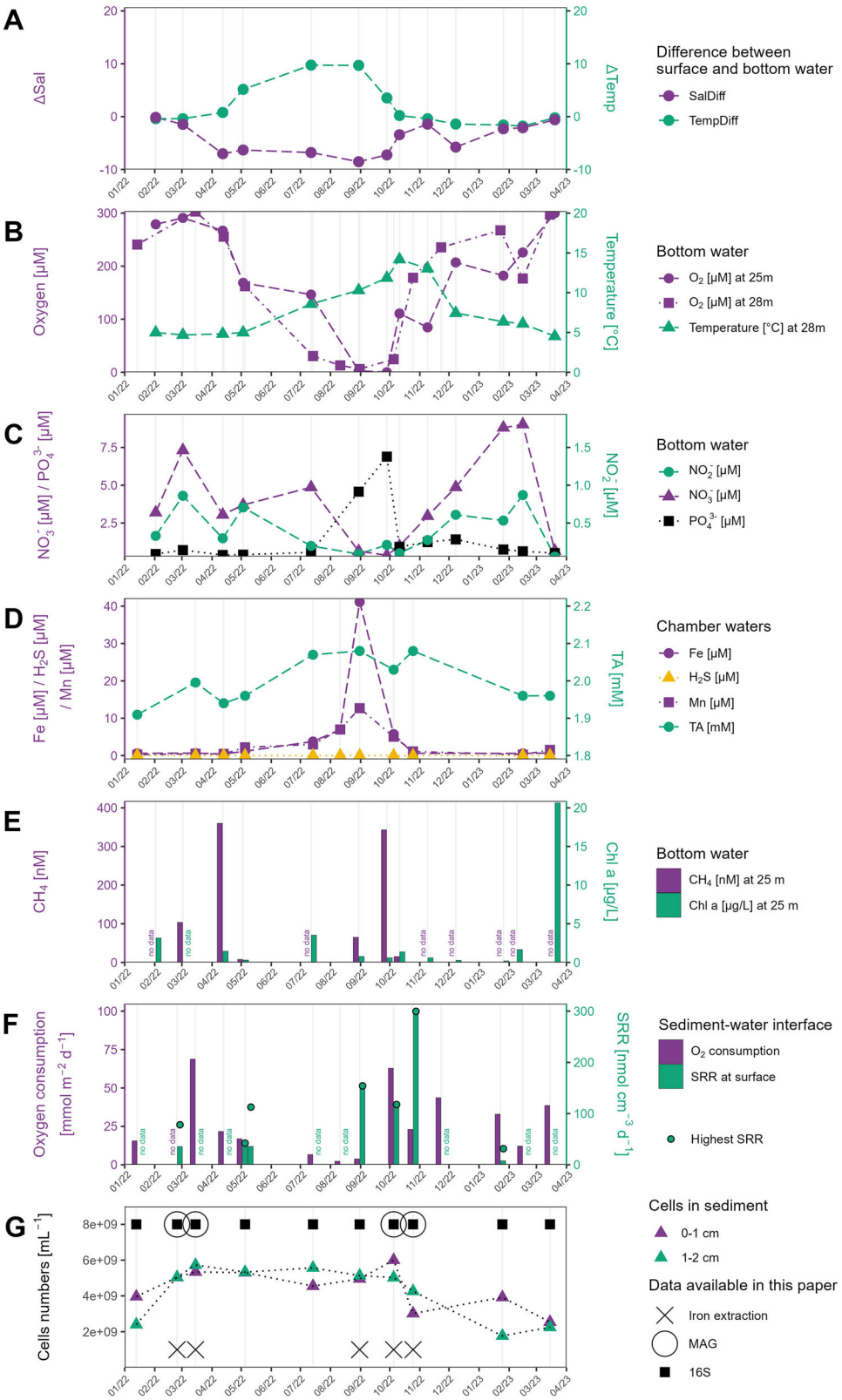


Fig. 1 | Water column properties and metabolic rates (January 2022 to March 2023). ΔTemp and ΔSal indicate surface to bottom water (25 m) temperature and salinity differences (**A**). Oxygen (O_2) was measured at 25 m via CTD; near the seafloor (28 m) O_2 and temperature (*T*) were monitored in-situ with a Unisense benthic minilander (**B**). Nitrate (NO_3^-), nitrite (NO_2^-), phosphate (PO_4^{3-}) were measured at 25 m water depth (**C**). Total iron (Fe), manganese (Mn), sulfide (H_2S) and alkalinity (TA) were determined from waters of an enclosed benthic chamber during 2-h incubations (**D**). Methane (CH_4) and chlorophyll a (Chl a) were from 25 m water depth (**E**). O_2 consumption rates were calculated from O_2 consumption during chamber experiments (**F**). Highest as well as surface sedimentary sulfate reduction rates (SRR) (**F**). Cell numbers for the top 0–1 cm and 1–2 cm and months for which Fe-extractions, metagenomic/transcriptomic as well as 16S rRNA amplicon analyses were conducted (**G**).

Assembled Genome (MAG) bins (Data S1), capturing diverse sulfur-cycling (*Beggiatoaceae*, *Desulfobacterota*), OM-degrading (*Planctomycetota*) and unclassified MAGs (40 bins). Read distribution analysis and mapping statistics revealed a complex, heterogeneous benthic community with a mix of bacterial, archaeal and eukaryotic contributors (Figs. S3 and S4, and Data S1–S4). Overall, the composition and transcriptional profile of each sample reflected shifts in metabolisms and community compositions between the months (Fig. S11A, B). Taxa peaked in abundance and activity during February/March, declined towards October, with only a few groups abundant late in the year (Fig. S3). The coefficient of variance (CV) across pathways of interest to this study showed that the metagenome abundances were stable across seasons (CV < 15%), but that metatranscriptomes shifted

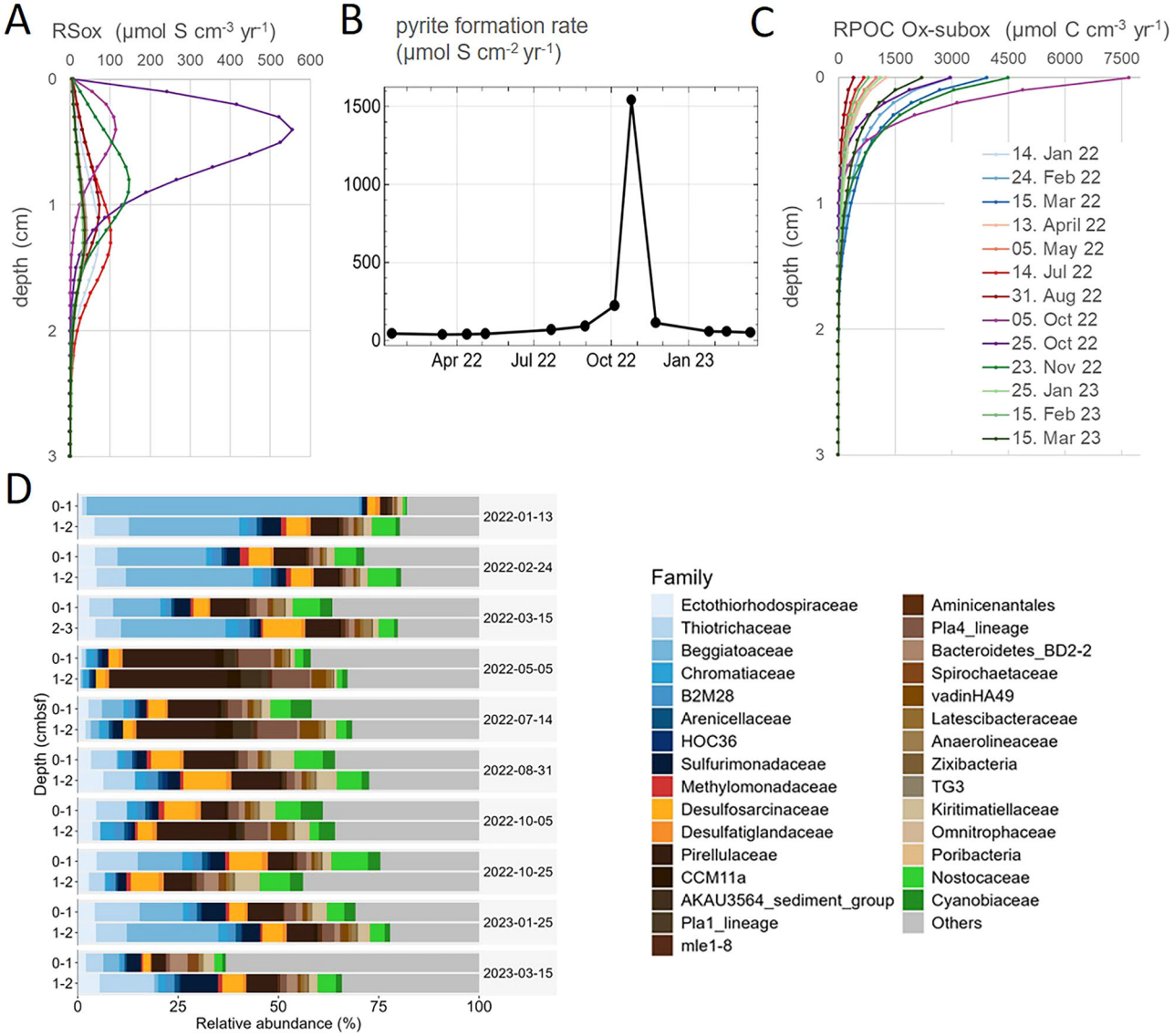


Fig. 2 | Modeled metabolic and pyrite production rates and microbial community shifts in the top 2 cm sediments. Modeled sulfide oxidation (Sox) along the sediment top 3 cm (**A**), modeled pyrite production rates derived from benthic chamber data for different months (**B**) and POC oxidation in the sediment top 3 cm under oxic-suboxic conditions (**C**) are shown. The 30 most abundant bacterial families are given for the 0–1 cm and 1–2 cm sediment depths for the different months (**D**). They are grouped by metabolism: SOB (blue), SRB (orange), methanotrophs (red), organotrophs (brown; excluding *Desulfobacterota*), cyanobacteria (green); "Others" (<30 families). For all 16S rRNA gene amplicon data see Fig. S7A–C.

in the microbial functions across seasons (CV > 15%) (Fig. 4). Principal Component Analysis (PCA) revealed a clear seasonal dichotomy where February/March communities were defined by carbohydrate active enzymes (CAZymes), Fe, nitrogen and oxidative sulfur cycling (Figs. S11C, D and S13C–E). In contrast, O_2 respiration was upregulated in early October surface sediments, accompanied by increasing SR in late October (Figs. S11D and S13D). Pathway enrichment analysis (FRY[30]) performed on the metatranscriptomes to identify significantly regulated KEGG modules[31] resolved their specific contributions to community metabolisms across seasons (Figs. 5 and S12, and Data S5–7):

Carbon (re)cycling

Transcriptomes revealed clear seasonal restructuring of carbon metabolism, marked by differences in extracellular enzyme activity, central metabolic pathways (e.g., Glycolysis and tricarboxylic acid (TCA) cycle) and autotrophic strategies (Figs. 4, 5, S11D, S12 and S13A, B). In February and/or March, genes for glycolysis, gluconeogenesis, C4-dicarboxylic acid cycle and formaldehyde assimilation pathways (RuMP—ribulose monophosphate and XuMP—xylulose-5-phosphate) were upregulated (Fig. 5). CAZymes involved in carbohydrate degradation, modification and synthesis[32] were also highly expressed in February/March, but both CAZymes and peptidases were downregulated in early and late October (Figs. 4 and S13A). Transcripts assigned to the CAZyme categories CE_xylan- and GH-α-rhamnoside were enriched in late October (Fig. S13A). Early October transcriptomes shifted toward upregulation of UDP-Glc biosynthesis, D-galactonate degradation, the pentose bisphosphate pathway and photorespiration (or glycolate "salvage" pathway), whereas late October transcriptomes upregulated the TCA cycle, pentose phosphate pathway, methylaspartate, glyoxylate cycle and ascorbate biosynthesis (Fig. 5). February transcripts associated with carbon recycling were largely attributed to *Beggiatoales,* whereas March and early October showed greater microbial diversity (Fig. S14A). Acetate oxidation was upregulated in February/March, downregulated in early October and upregulated again in late October (Fig. 4). The associated transcripts were primarily affiliated with SRB, mainly *Desulfatiglandales* and *Desulfobacterales* in February/March and early October and late October transcripts were almost exclusively

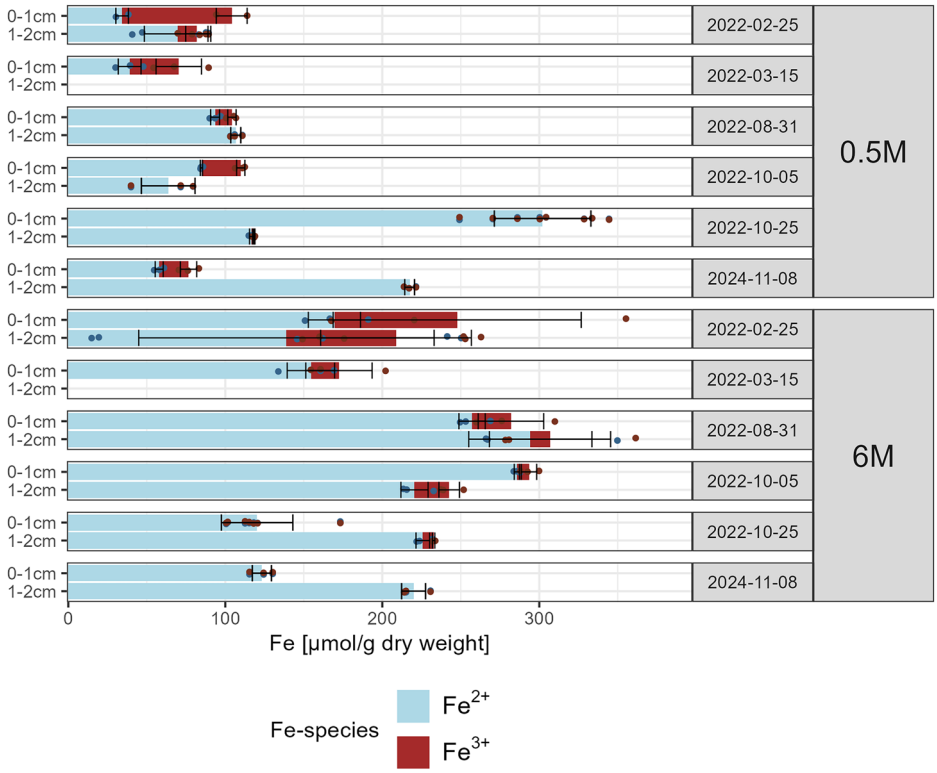


Fig. 3 | Sequential Fe extractions for near surface sediments for February, March, late August, early and late October 2022 and November 2024. Stacked bars show mean Fe(II) and Fe(III) concentration in the 0.5 M and 6 M fractions, with Fe(II) shown in light blue and Fe(III) in brown. Individual points represent the values of the respective technical replicates. Error bars represent ± SD of technical replicates ($n = 3$), except for 25 February 2022 (1–2 cm), for which $n = 6$ for both the 0.5 M and 6 M extractions; 25 October 2026 (0–1 cm), for which $n = 7$ for the 0.5 M and 6 M and 25 February 2022 (0–1 cm) were $n = 2$.

assigned to *Desulfatiglandales* (Fig. S14B). Gene expression of autotrophic CO_2 fixation pathways responded to seasonal redox potential (Fig. 5). February transcriptomes were enriched in genes associated with the C4-dicarboxylic acid cycle and the Calvin-Benson-Bassham (CBB) cycle (Figs. 5 and S13B). By March, transcripts of the WL pathway were upregulated, which coincided with enrichment of *Desulfobacterales* and unclassified Archaea (Fig. S14C). During re-ventilation in early October, the dicarboxylate-hydroxybutyrate (DC-HB) cycle emerged. By late October, upregulation of the incomplete reductive citrate cycle (irTCA) was observed (Fig. 5).

Nitrogen metabolism

February and especially March sediments exhibited the highest transcript abundances associated with NO_3^- reduction to NO_2^-, with transcripts primarily linked to *Beggiatoaceae* and unclassified Bacteria (Figs. 6A and S13D). In March, denitrification appeared intensified, given transcript enrichment for the reduction of nitrous oxide to dinitrogen. In October, no considerable upregulation of the nitrogen cycle was identified (Fig. S13C).

Sulfur metabolism

The sulfur cycle displayed distinct transcriptional profiles between months (Figs. 6B and S13E). In February/March, surface sediments and transcripts were largely attributed to intracellular sulfur oxidation and putative sulfur transferase activity. Although genes from *Beggiatoaceae* were detected in both metagenomes and metatranscriptomes, no genes related to *Beggiatoaceae*'s sulfur oxidation pathway were found[33]. The majority of genes upregulated in February/March were associated with *dsrE/dsrF* of unclassified Bacteria, some *Gammaproteobacteria* and SRB (Figs. 6B, S13D and S14E). Upregulated *aprA* genes in early October were affiliated with *Gammaproteobacteria*, SRB, and unclassified Bacteria; those of late October were primarily affiliated with SRB as well as unclassified Archaea (Fig. S14E).

Metal cycling

Genes encoding for Fe cycling in metagenomes are detailed in Text S6. Expression of *omcS* was highest in March, with lower but somewhat similar levels observed in February and early October, but declined sharply by late October (Figs. 6C and S13E). Yet, upregulation of genes known to be associated with Fe-oxidation could not be detected. March exhibited the highest and early October slightly elevated transcript abundances of genes related to Mn-oxidation (Fig. 4).

Community growth and stress strategies

Pathway enrichment analysis (FRY) identified distinct transcriptional shifts in stress and growth-related modules between seasons (Fig. 5). In February, transcripts for vancomycin resistance were significantly upregulated compared to October. Conversely, early October samples showed downregulation of fatty acid and amino acid biosynthesis pathways, specifically the ornithine–urea cycle and isoleucine biosynthesis relative to March. However, when compared to the spring months, both early and late October samples exhibited strong upregulation of biosynthesis pathways for nucleotides and cofactors, including NAD, thiamine and heme. Transcripts for aerobic or anaerobic methane oxidation and methanogenesis were not detected.

Discussion

Seasonal cycle and potential interactions

Although coastal sediments cover only a small fraction of the seafloor, they are dynamic biogeochemical hotspots, accounting for >80% of global marine carbon mineralization and burial[34] and are thus highly relevant as carbon sinks and sources. Microbial communities mediate OM breakdown from complex polymers to simple fermentation products, driving a cascade of aerobic to anaerobic processes such as Mn-, Fe- and SR and methanogenesis[22,34,35]. Hence, carbon, nitrogen, metal and sulfur cycling are closely interlinked, with O_2 availability, redox conditions and temperature regulating the pace and products of microbial activity[24,27,29]. Consequently, sediments act as both sinks and sources for key compounds[36–38], with strong regulatory feedback for the overlying water column. Below, we discuss seasonal variability of these benthic processes and microbial communities at Boknis Eck, focusing on the surface 0–1 cm sediment layer.

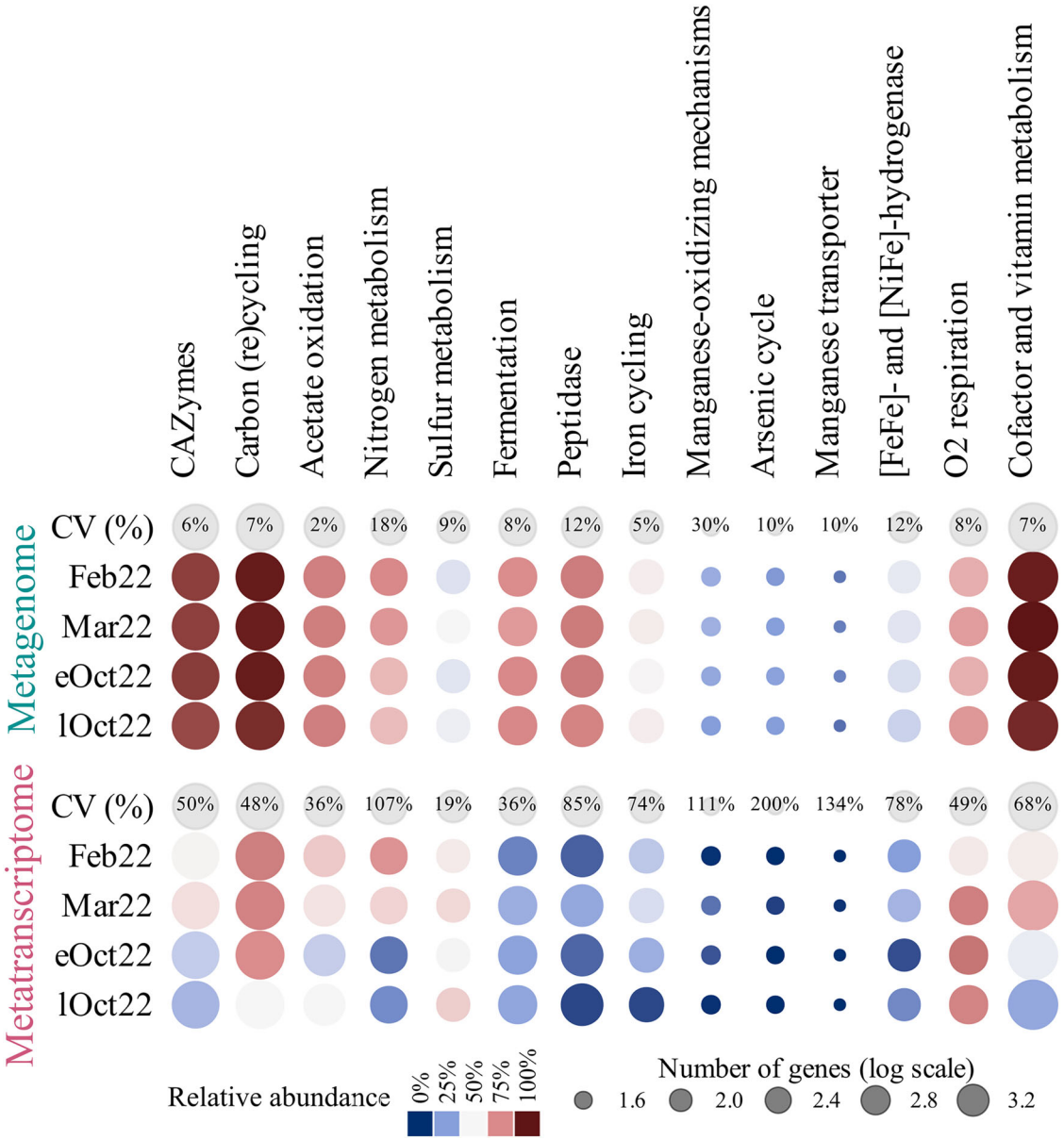


Fig. 4 | Comparison of genomic potential and transcriptional activity across seasons. Bubble plot displaying the normalized relative abundance (color gradient) and total gene count (circle size, log scale) for key metabolic functional categories in the metagenome (top) and metatranscriptome (bottom). The Coefficient of Variation (CV %) is listed for each category to quantify seasonal variability (Standard Deviation/Mean). The data reveals a distinct decoupling: while the genomic potential remains stable across seasons (low CV, ≤30%), the transcriptional activity exhibits high plasticity (high CV, up to 200%).

Well mixed water column at low temperatures (January–March)

During late winter, when bottom waters were cold (4 °C), well-mixed and nutrient-rich (Fig. 1A–C), high bottom water O_2 concentrations kept SRR beneath the sediment surface low (Fig. 1F), allowing for sulfide to accumulate (>1 mM) only below 5 cm sediment depth (Figs. 7 and S8). In January 2022, SOB dominated the sediment-water interface (Fig. S10A, B). Following the February algal bloom and a fresh OM flux to the seafloor, SOB and modeled S_{ox} rates declined, while cell numbers and organotrophic Bacteria, primarily *Planctomycetota*, increased (Figs. 1G, 2A, D and S3). *Beggiatoaceae* and other SOB in late winter were likely sustained by sulfide originating from deeper sediments, reflecting conversion of older OM (Fig. S14D). Metatranscriptomes confirmed that sulfur oxidation via free available sulfide was not a dominant process (CV = 19%; Fig. 4). Instead, the increased expression of *dsrE/dsrF* (Figs. 6B, S13D and S14E) may indicate a greater reliance on intracellularly stored sulfur[39] under conditions of limited sulfide in the upper sediment porewaters (Fig. S8). Transcripts associated with SR were rather limited, coinciding with low SRR (Figs. 1F, S8 and S14D). In late winter, sulfur-oxidizing mechanisms based on stored sulfur appeared more prominent in the top sediment than sulfur-reducing processes.

Upregulation of glycolysis (KEGG modules M00001, M00002 in Fig. 5), C4-dicarboxylic acid cycle (KEGG modules M00171, M00172 in Fig. 5) and gluconeogenesis (KEGG module M00003 in Fig. 5) in February sediments posited glucose synthesis and use of alternative carbon sources such as C4 acids, reflecting conditions of limited labile OM contents prior to the algal bloom. Fresh POC depositions in February 2022 then induced a shift in the surface microbial community as documented by increasing modeled sedimentary $POC_{ox\text{-}subox}$ degradation rates from January to March (Figs. 1E and 2C). This suggested that freshly deposited OM was primarily degraded via oxic and suboxic pathways. Yet, upregulation of the WL pathway and the presence of distinct anaerobes implied the existence of anoxic micro-niches, possibly generated by intense respiration of bloom-

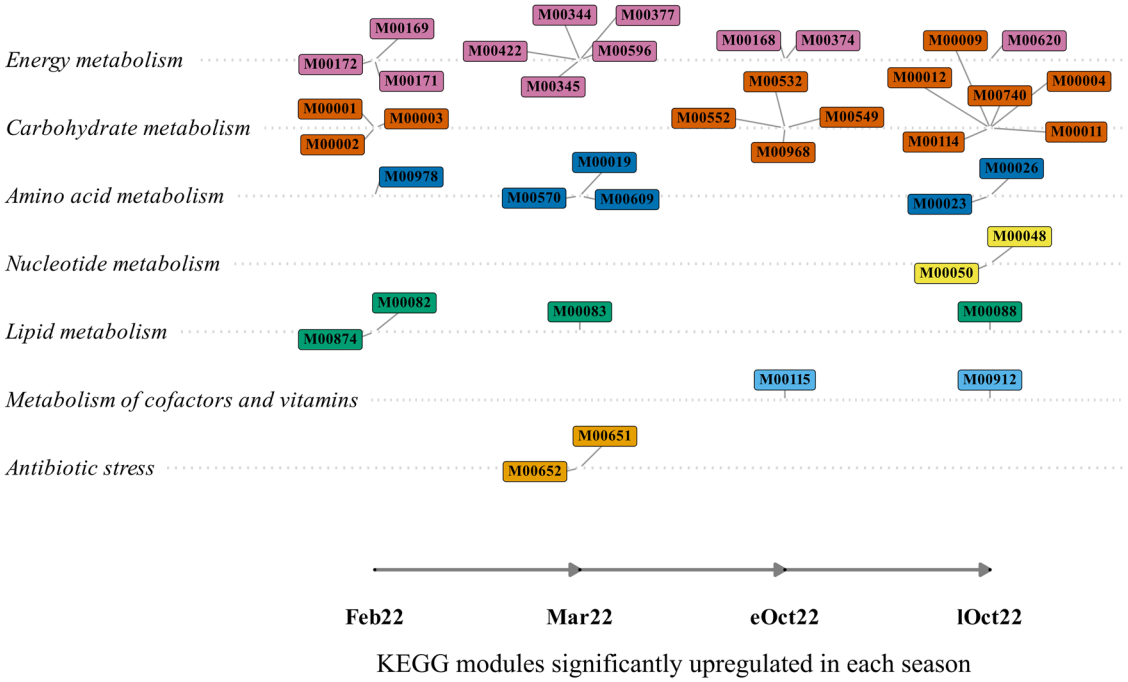


Fig. 5 | Seasonal pathway enrichment in microbial metatranscriptomes. Significantly upregulated pathways ($P \leq 0.05$) were identified using FRY gene set enrichment analysis and assigned to the season exhibiting their highest relative expression. Modules are spatially organized by functional category (*y*-axis) and temporal dominance (*x*-axis), revealing a progression from energy and carbohydrate metabolism in Feb-March to nucleotide and cofactor biosynthesis in October. Abbreviations are for energy metabolism: C4-dicarboxylic acid cycle (M00171, M00172), Calvin–Benson–Bassham (CBB) cycle (M00169), reductive acetyl-CoA (Wood-Ljungdahl) pathway (M00377), dissimilatory sulfate reduction represented by *dsrEF* (M00596), Acetyl-CoA pathway (M00422), formaldehyde assimilation pathways (RuMP – ribulose monophosphate; M00345 and XuMP – xylulose-5-phosphate; M00344), dicarboxylate-hydroxybutyrate (DC-HB) cycle (M00374), Crassulacean acid metabolism (M00168), incomplete reductive citrate cycle (irTCA) (M00620). Carbohydrate metabolism: glycolysis (M00001; M00002), Gluconeogenesis (M00003), UDP-Glc biosynthesis (M00549), D-galactonate degradation (M00552), Pentose bisphosphate pathway (M00968), pentose phosphate pathway (M00004), Photorespiration (M00532), tricarboxylic acid (TCA) cycle (M00009), methylaspartate (M00740), glyoxylate cycle (M00012), Citrate cycle (M00011), Ascorbate biosynthesis (M00114). Amino acid metabolism: Ornithine-ammonia cycle (M00978), ornithine–urea cycle (M00609), Valine/isoleucine biosynthesis (M00019), isoleucine biosynthesis (M00570), Tryptophan biosynthesis (M00023) and Histidine biosynthesis (M00026). Nucleotide metabolism: De novo purine biosynthesis (M00048), Guanine ribonucleotide biosynthesis (M00050). Lipid metabolism: Fatty acid biosynthesis (M00082, M00083, M00874), Ketone body biosynthesis (M00088). Metabolism of cofactors and vitamins: NAD (M00115, M00912). Antibiotic stress: vancomycin resistance (M00651, M00652).

derived OM by e.g. co-occurring *Woeseiales* populations cf[40] (Figs. 1 and S14C). The combined availability of labile OM and O_2 at the seafloor was reflected in measured high benthic in-situ O_2 consumption rates in March (Fig. 1) and supported a high microbial competition (Fig. 5) with diverse functions evident from numerous upregulated genes encoding for carbon, nitrogen, metal and sulfur cycling (Figs. 4 and 6). To maximize OM degradation, surface sediment microbial communities expanded their metabolic repertoire from February to March, with upregulation of CAZymes and peptidases (hydrolysis), glycolysis and fermentation and anaerobic respiration (Figs. 4–6). Anaerobic respiration appeared dominated by NO_3^-- and Fe- reduction, with enhanced nitrogen turnover in late winter and a transition to more reduced forms from February to March.

Oxic conditions in deep waters preserved Fe-(oxyhdr)oxides in surface sediments (Fig. 3), allowing for enhanced microbially mediated dissolution of Fe(III)-bearing minerals as indicated by upregulated *omcS*[41] (Figs. 6C, S8 and S13E) and efficient re-precipitation at the sediment-water interface (Figs. 1D and S6). Likewise, elevated dissolved Mn concentrations in late winter porewaters posited Mn-mineral dissolution (Figs. S6 and S8), and exploitation by manganese oxidizers (cf. Fig. 4). Transcript abundance confirmed enhanced capacity of the local benthic microbial communities to consume hydrogen (Figs. 4 and S14F) and assimilate formaldehyde (Fig. 5); the latter was produced via oxidation of methane, methanol and methylated compounds released via stepwise OM degradation[25,42–45]. This would suggest highly active microbes that are efficiently utilizing intermediates of OM degradation. However, molecular functional analysis did not confirm canonical microbial methane oxidation in sediments (Fig. S10), despite elevated methane concentrations in March 2022 deep waters (Fig. 1E). This may be related to limited transcriptome coverage or to the fact that genes involved in methane oxidation were not detected due to incomplete or insufficient functional annotation.

Ongoing oxygen depletion and increasing water temperatures (May–July)

Water column stratification strengthened, leading to increasingly O_2-depleted bottom waters, while NO_3^- remained available (Fig. 1). Markedly reduced in-situ benthic O_2 consumption and lower modeled $POC_{ox\text{-}subox}$ degradation rates in May (Fig. 2C) suggest that labile OM derived from the late winter bloom was largely exhausted. Consequently, the benthic microbial community would become increasingly sustained by less labile and more refractory OM. This transition was accompanied by a shift in the benthic microbial community likely responsible for these altered mechanisms: *Planctomycetota*, mostly *Pirellulaceae*, became enriched in surface sediments, while SOB and canonical SRB declined (Fig. 2D). *Pirellulaceae* possess a broad repertoire of CAZymes enabling them to hydrolyze complex carbon polymers[46,47], including sulfatases cleaving sulfated heteropolysaccharides[48], a substrate otherwise inaccessible to OM degraders. Together with *Pirellulaceae's* slow growth rates and low carbon and nitrogen demand[49], these traits likely conferred a competitive advantage under labile OM-limited conditions in May sediments. Detected *Planctomycetota* included both initial degraders of carbohydrate-rich POC (phytoplankton, plant material) and those utilizing secondary POC remineralization products, e.g., proteins and acetate[49–53]. Additionally, some

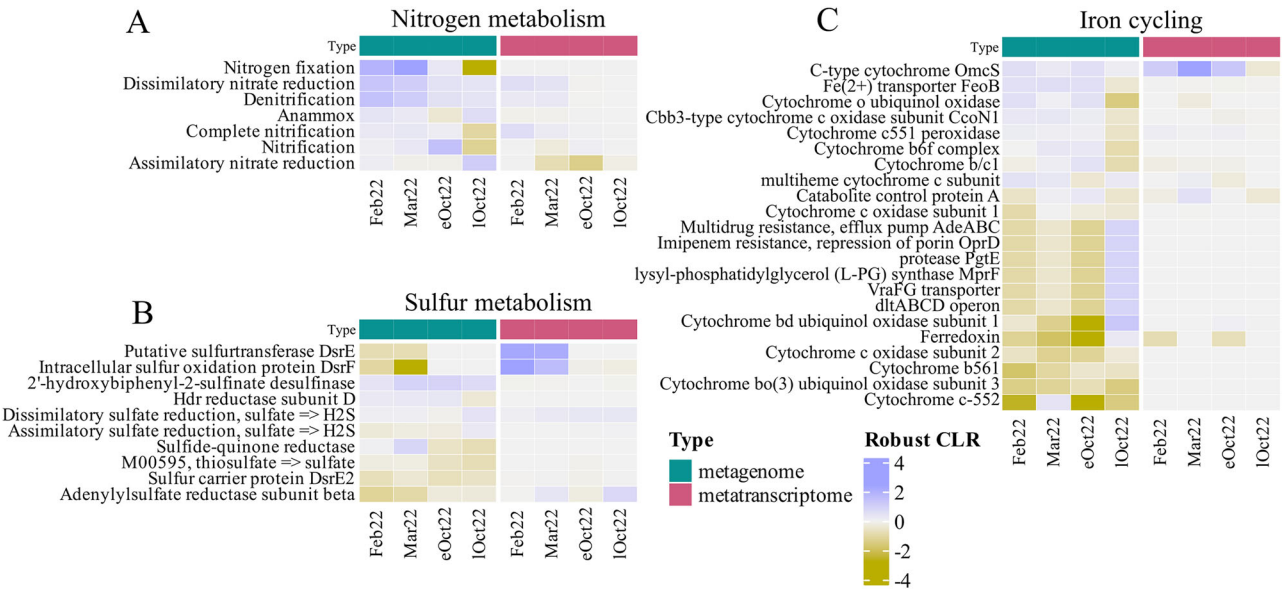


Fig. 6 | Comparison of functional profiles related to nitrogen metabolism, sulfur metabolism and iron cycling in metagenomes and metatranscriptomes. Heatmaps showing Robust CLR-transformed abundances of KEGG modules associated with nitrogen metabolism (**A**), sulfur metabolism (**B**) and iron cycling (**C**) in metagenomic (left panels, green) and metatranscriptomic (right panels, magenta) datasets.

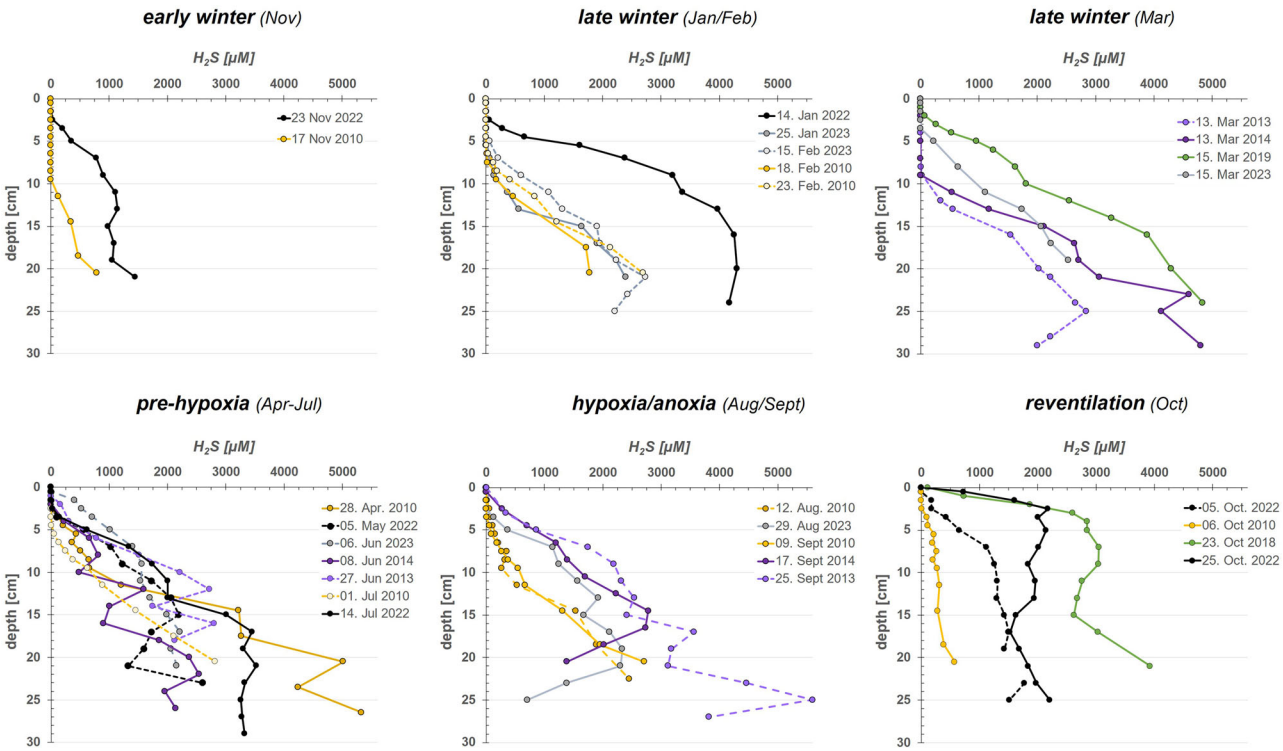


Fig. 7 | Historic[12,17,71] and current sulfide concentrations of sediment porewaters for the different seasons at Boknis Eck illustrate shallowing of sulfide enrichments in porewaters since 2010. The different years are color coded, where historic data from 2010 is in yellow, from 2013 and 2014 in purple shades, 2018 and 2019 in green and recent data from 2022 and 2023 in grey and black, respectively.

of the enriched *Pirellulaceae* groups catalyze carbohydrate fermentation and sulfur reduction[54] adding to further metabolic flexibility required in the system under these conditions. Given slower OM breakdown, its end product, methane, was barely measurable close to the seafloor in May (Fig. 1E), aligning with the absence of known anaerobic methane oxidizers in sediments (Fig. S10C).

In July, near-bottom waters became warmer and hypoxic (30 µM O_2), resulting in reduced in-situ benthic O_2 consumption rates reaching ~10% of March levels (Fig. 1B). Ongoing bottom water deoxygenation would impose considerable constraints on the activity of sediment-dwelling invertebrates (meio- and macrofauna), restricting O_2 transport and reactive solute /particle exchange between bottom waters and surface sediments[12,28,29],

providing grounds for sulfide enrichments. The proposed limited bioirrigation matched modeled suppressed $POC_{ox\text{-}suboxic}$ degradation (Fig. 2C). Continued O_2-depletion of deep waters and a renewed OM-flux to the seafloor in July (Fig. 2E) triggered a further benthic microbial community shift. This was reflected in *Pirellulaceae* declining in top 0–1 cm sediment layer, while other organotrophic Bacteria and SOB increased (Figs. 1E and 2E). Under these conditions, SOB made up 20% of near-surface bacterial gene amplicons, congruent with higher modeled S_{ox} rates (Fig. 2A, E). Since nitrate was still abundant in deep waters (Fig. 1C), NO_3^--storing *Beggiatoaceae* likely acted as temporary effective sulfide filters[33,55], since their vertical occurrence aligned well with sulfide kept near zero in the depth horizons they colonized (Figs. 2D, S8 and S10A).

Anoxia and rising temperatures (August-September)

End of August, rising temperatures and intensified water column stratification exacerbated severe depletion of bottom water O_2 (7 μM) and NO_3^- (0,6 μM) (Fig. 1). Consequently, measured benthic in-situ O_2 consumption and modeled $POC_{ox\text{-}subox}$ degradation rates reached their annual minimum (Figs. 2B and S4). Surface sediments still remained dominated by abundant organotrophs, mostly *Planctomycetota* and SRB, highlighting the shift towards microbial utilization of OM via metabolic pathways independent of O_2 and NO_3^- as terminal electron acceptors. During these suboxic (<10 μM O_2) bottom waters, OM decomposition would shift from aerobic to less efficient anaerobic metabolisms[18,20,21,56], generating secondary degradation products like volatile fatty acids and hydrogen, oxidized by SRB[57] and methanogens[58], releasing sulfide and methane, respectively. POC degradation would become slower and less efficient[56], while remaining dissolved organic carbon (DOC) would exhibit greater reductivity and bioavailability[59] - once O_2 became available again later in the year. In line with these processes, SRR sediment surface maxima were ~2-fold higher in late August than in February/March (Fig. 1F). This increase likely reflected higher abundance of SRB (Figs. 2D and S10A) and temperature accelerated SR[24,60,61]. With other electron acceptors depleted in bottom waters (Fig. 1B, C), SR-dominated surface sediments (Fig. 1F) and fostered sulfidic conditions. Sequential Fe-extractions indicated solid-phase Fe was mainly present as Fe(II) with little mineral-based Fe(III) available for OM degradation (Fig. 3). Reductive dissolution of P-bearing Fe- and Mn-minerals under sulfidic conditions together with ongoing OM re-mineralization[12,62] likely drove sedimentary PO_4^{3-}, Fe and Mn release into the water column (Figs. 1C, D and S6). Mobilized Fe would react with biologically produced sulfide to form FeS and FeS_2 in the sediments[36–38], hindering benthic sulfide release. Silica concentrations increased toward the sediment surface under anoxia (Figs. 1D and S3), probably reflecting diatom frustule dissolution as seen in O_2-deficient waters[63]. By late September, bottom waters had become anoxic, accompanied by high methane concentrations (Fig. 1E).

Re-ventilation and peak temperatures (October-November)

In October, water column stratification started breaking up, leading to progressive re-ventilation of bottom waters (Fig. 1) and triggering further shifts in benthic microbial metabolisms (Figs. 4–6). Early October represented a critical transient phase where O_2 availability in bottom waters increased (Fig. 1B), but sediments remained highly reduced (Fig. S8). A rapid stimulation of aerobic respiration coupled to OM degradation (Fig. 4) during deep-water re-oxygenation in early October was reflected in some of the highest annual in-situ benthic O_2 consumption rates, modeled $POC_{ox\text{-}subox}$ degradation rates (Figs. 1F and 2C), upregulation of O_2 respiration and central carbon metabolisms (Figs. 4, 5 and S11D). This response was likely driven by fresh O_2 supply and bioavailable organic carbon accumulated during anoxic conditions[59], further amplified by the highest annual temperatures[29,64]. Within this changing environmental context, October transcriptomes suggested a reorganization of carbon metabolism following the onset of fall re-ventilation. Early October was marked by reduced expression of CAZymes, peptidases and acetate oxidation (Figs. 4, 5 and S11D), pointing towards a reduction in the degradation of complex OM, particularly polysaccharides. Instead, the upregulation of D-galactonate degradation suggested utilization of more readily available carbohydrate-derived substrates, while increased expression of UDP-glucose biosynthesis, the pentose bisphosphate pathway and photorespiration indicated continued metabolic activity within carbohydrate metabolism (Fig. 5). In late October increased expression of TCA cycle, pentose phosphate pathway, glyoxylate cycle and methylaspartate cycle transcripts (Fig. 5), renewed acetate oxidation (Fig. 4) and the selective enrichment of the CAZyme categories CE_xylan and GH_α rhamnoside (Fig. 13A) posits a further reorganization of carbon metabolism. Together with elevated alkalinity and NH_4^+ concentrations, these late October transcriptional patterns were consistent with continued remineralization and an increased capacity for acetate oxidation and the processing of C2 intermediates through central metabolic pathways.

Despite increasing re-oxygenation of deep waters, the highest annual SRR maxima were measured in October (Fig. 1F), suggesting some decoupling between immediate changes in deep-water conditions and benthic metabolisms. From early October to late October, surface near SRR, sulfide accumulation, modeled S_{ox} rates and FeS_2 formation progressively increased (Figs. 1F, 2A, B and S8). The increasing shallow sulfide accumulation between early and late October altered microbial metabolism and abiotic reactions: While some upregulated sulfur-cycling genes (*aprA*) in early October were affiliated with sulfur-oxidizing taxa[39], those detected in late October were predominantly affiliated with taxa commonly linked to SR[65] (Figs. S13D and S14E). Although the latter stands in contrast to the modeled annual peak S_{ox} rates in late October, the upregulation of *aprA* in unclassified Archaea (~17% of upregulated *aprA* genes) may indicate active sulfur oxidation in late October (Fig. S14E, and Data S7). This highlights our limited understanding of the metabolic potential of the uncultured microbial majority[66]. Alternatively, it is also possible that the complex sulfur cycle was not adequately represented and parameterized in the model.

Fe and Mn cycling reflected the legacy of the sediments' previous exposure to O_2-deficient waters. In early October, microbial Mn-oxidation kept dissolved Mn low, while by late October sulfide-driven Mn-oxide dissolution caused Mn^{2+} accumulation as microbial Mn-oxidation ceased (Figs. 4 and S8)[67], limiting regeneration of the reactive Mn-pool. Reduced Mn-oxide availability for sulfide oxidation likely facilitated sulfide accumulation in porewaters[67]. Initial re-ventilation of bottom waters in early October also led to temporary enrichment of reactive Fe(III)-minerals in surface sediments (Fig. 2). Given abiotic and biotic reactions, Fe(III)-minerals dissolved in early October (Figs. 6C and S8). This, however, did not sustain microbial Fe re-oxidation (Fig. 6C), but instead reduced Fe reacted with accumulated sulfide to form Fe-S minerals (Figs. 2B and S8). This was accompanied by a drop in cell numbers, exhaustion of the Fe(III)-pool, absence of transcripts associated with Fe-redox reactions, sulfidic conditions and considerably promoted FeS_2 formation at the sediment surface (Figs. 1G, 2B, 3, 4, 6 and S8), implying that Fe-cycling was strongly controlled by sediment redox conditions. Abiotic sulfide removal via FeS_2 formation gradually dominated benthic oxidative sulfur cycling during water column re-oxygenation, peaking by late October. Overall, these data suggest tight coupling between reductive and oxidative sulfur, Fe and Mn cycling in October, with a shift from biological to abiotic controls and intense sulfide enrichment in surface sediments.

A distinct anabolic strategy emerged when comparing October to March. In October, we observed a strong upregulation of biosynthesis pathways for generating cell building blocks, including nucleotides (deoxyribonucleotide and pyrimidine biosynthesis) and vitamins/cofactors (NAD, thiamine, and heme biosynthesis) (Fig. 5), critical for microbial growth or niche shifts[68–70]. This upregulation aligned with high cell counts in the surface sediment in early October (Fig. S6), indicating that, despite hypoxia, the community maintained substantial growth potential. Critically, the upregulation of NAD biosynthesis from aspartate and tryptophan in October serves a dual purpose. Beyond growth, NAD^+/NADH balance is vital for redox reactions and managing intracellular reactive oxygen species[35]. This shift likely reflects a stabilizing mechanism for intracellular

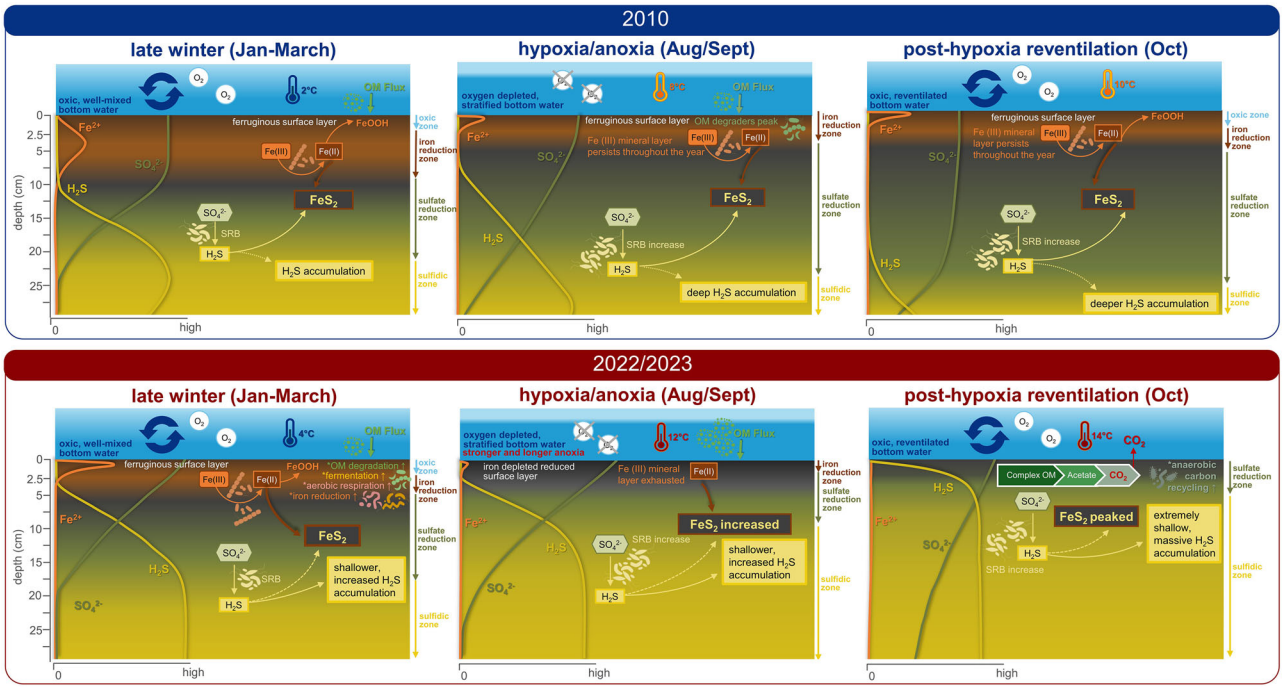


Fig. 8 | Conceptual model of the seasonal transition from a ferruginous to a progressively sulfidic sediment system at Boknis Eck in the southwestern Baltic Sea between 2010 and 2022/2023. Seasonal biogeochemical dynamics at Boknis Eck in late winter (January–March), summer hypoxia/anoxia (August–September) and post-hypoxia re-ventilation (October) are compared between 2010 (top) and 2022/2023 (bottom). The conceptual model is based on observations from this study and previously published data for 2010[12,15,71,91]. Curves schematically illustrate the depth distributions of dissolved H_2S, SO_4^{2-} and Fe^{2+}. In 2010, a reactive Fe(III)-mineral layer persisted throughout the annual cycle, maintaining the sediment's iron-buffering capacity despite seasonal O_2 depletion. Consequently, sulfide accumulation remained restricted to deeper sediment layers and retreated following autumn re-ventilation. By contrast, in 2022/2023 the reactive Fe(III)-mineral pool became exhausted in summer and led to the sulfidic zone progressively expanding towards the sediment-water interface. Although bottom waters became re-oxygenated during autumn, sulfide remained stored within surface sediments, indicating incomplete recovery of sediment redox conditions. Metatranscriptomic analyses (only for February, March, early and late October 2022) further revealed a seasonal transition from enhanced aerobic respiration, organic matter degradation, fermentation and iron reduction during late winter to anaerobic carbon recycling after hypoxia, demonstrating that microbial metabolism remained dominated by anaerobic processes despite bottom-water re-oxygenation. Together, these observations illustrate a transition from a seasonally buffered ferruginous sediment system in 2010 to a substantially weakened iron-buffering capacity and a progressively more persistent sulfidic state in 2022/2023.

redox homeostasis in response to the changing O_2 availability at the sediment surface.

Taken together, these results show that deep-water re-oxygenation during early re-ventilation did not "re-set" sediment biogeochemistry to the winter state but initiated a brief phase of intensified aerobic metabolisms superimposed on a highly reduced sediment matrix. Consistent with observations from other seasonally hypoxic marine systems, these findings indicate that sediment recovery lags behind bottom water re-oxygenation, since continued anaerobic metabolisms and slow regeneration of reactive Fe and Mn minerals sustain reducing conditions in surface sediments after oxygen has returned to bottom waters[23,28].

Declining sediment resistance under persistent seasonal deoxygenation. The study suggests a progressive loss of sedimentary resiliance at Boknis Eck under sustained seasonal deoxygenation (Fig. 8). During the annual cycle 2022, surface sediments transitioned from oxic or ferruginous to sulfidic conditions (Figs. 2B, 6C, S8 and S13E). Shallow sulfide enrichments (up to 700 µM in the top 1 cm sediments) indicated that Fe-cycling no longer buffered sulfide accumulation by summer. In late August 2023, sulfide release from sediments was observed (Fig. S15), further suggesting that nowadays by late summer, sediment sulfide retention capacity appears to have become exhausted. The seasonal dynamics are consistent with the long-term evolution of the system. In 2010, dissolved Fe^{2+} was enriched in porewaters of near-surface sediments almost year-round, while sulfide accumulation was confined to deeper layers[12,71] (Fig. 7). Based on these data, sulfide production and benthic FeS_2 formation were predicted to be slower than overall reductive Fe-dissolution[12], indicating that in 2010 Fe(III)-minerals largely persisted throughout the year. The shift from year-round oxic or ferruginous (2010) to temporary sulfidic (2022, 2023) surface sediments in late summer likely reflects temporally and spatially expanded O_2-depleted bottom waters[10], diminishing or delaying Fe re-oxidation while benthic sulfide production shallows as deep-water hypoxia resumes (Fig. 8). Fe-oxide availability, though, remains crucial, as these minerals sequester toxic sulfide in subsurface sediments during anoxia[28].

At Boknis Eck, rising temperatures, intensified stratification and bacterial biomass production coincide with more frequent and prolonged deep-water deoxygenation[10,15,29]. The 2022/2023 seasonal cycle exemplifies how warming and O_2-depletion stimulate benthic anaerobic metabolisms, sulfidic conditions and increased long-term sequestration of reactive Fe as Fe-S-minerals[27,72], progressively reducing sedimentary resilience. Together, porewater chemistry, Fe-mineral speciation, measured and modeled metabolic rates and transcriptomic data indicate a transition toward self-reinforcing hypoxia feedbacks that amplify deoxygenation (Fig. 8). The seasonal biogeochemical dynamics at Boknis Eck may thus represent an early stage in the development of persistently anoxic coastal ecosystems. This trajectory is consistent with perennially anoxic ecosystems like the deep Baltic or Black Seas, where persistent O_2 depletion has selected for anaerobic microbial communities and ecosystem functioning dominated by SR, methanogenesis and methane cycling[23,73,74]. This ongoing transition at Boknis Eck may well further restructure microbial community compositions and function, while weakening benthic Fe buffering and facilitating benthic sulfide release. As a result, increased nutrient release to the water

column may stimulate primary production, reinforce hypoxia and ultimately reduce the resilience and ecological health of this coastal ecosystem.

Materials and methods

Seawater and sedimentary properties were determined for Boknis Eck (Eckernförde Bay, SW Baltic Sea, Germany) between January 2022 and March 2023 on a near monthly basis. A map and coordinates of individual stations are given in Fig. S1 and Data S8.

Seawater and sedimentary properties

Water-column samples were collected with a CTD/rosette system equipped with Niskin bottles to determine temperature, O_2, salinity and dissolved nutrients. Chlorophyll a (Chl a) and methane (CH_4) concentrations were measured in the water column. Sediment cores were collected using a multicorer. Sediment samples were sectioned at a resolution of 1 cm intervals in the upper 4 cm and 2 cm intervals below. Sediment samples were analyzed for porosity, porewater chemistry, microbial abundance, microbial community composition and gene expression. Detailed sampling procedures and analytical protocols are provided in the Supplementary Materials and Methods Text 1. Sequential Fe-extractions quantified poorly crystalline (0.5 M HCl-extractable) and crystalline (6 M HCl-extractable) Fe(II) and Fe(III). Due to limited sediment availability, the same frozen samples were used for both RNA and Fe analyses. Samples were thawed once, briefly subsampled for RNA under ambient laboratory conditions, and immediately refrozen prior to sequential Fe extraction. Although this procedure may have caused some oxidation of reactive Fe(II) phases, potentially leading to an overestimation of Fe(III), all samples were handled identically. Consequently, comparisons among treatments and sampling months remain valid, whereas absolute Fe(III) abundances should be interpreted with some caution.

Measured and modeled metabolic rates

Benthic chamber incubations were carried out using a MiniChamber Lander system (Unisense, Aarhus, Denmark). A set of optodes monitored O_2 and conductivity, while a miniaturized amperometric sensor was used to measure hydrogen sulfide in bottom waters. O_2 sensor data were used to calculate benthic O_2 consumption rates via linear regression. Water samples were taken in situ at three time points during 2-h incubations using a syringe sampler for further analyses. SR rates (SRR) were quantified by the whole-core-injection-method[75]. Porewater data were evaluated using reactive transport modeling to calculate rates of oxic/suboxic POC degradation ($POC_{ox\text{-}subox}$), sulfide oxidation (S_{ox}), SRR and pyrite (FeS_2) formation in anoxic sediments[12,17]. Details on measured metabolic and modeled rates are given in Texts S2 and S3, respectively.

Microscopy and 16S rRNA gene amplicon analyses

Cell numbers were determined by DAPI staining and microscopy of sediment samples that were fixed in formaldehyde and concentrated on polycarbonate filters. To assess the active microbial community, total RNA was extracted from ~500 mg sediment, transformed into cDNA and 16S rRNA bacterial and archaeal gene amplicon libraries were generated. Sequencing was performed on an Illumina MiSeq platform (2 × 300 bp, paired-end). Further information is in Text S4.

Metagenomic and transcriptomic analyses

DNA and RNA of the 0–1 cm sediment horizons from 24. February, 15. March, 05. October and 25. October 2022 was extracted in triplicate. Using the NucleoBond® RNA Soil Mini Kit in combination with the NucleoBond® DNA Set (Macherey-Nagel, Düren, Germany), following the manufacturer's protocols. For DNA sequencing, the 3 parallels of each sample were pooled, while the RNA triplicates were processed individually. Metagenomic sequencing libraries were constructed using the NEBNext Ultra II FS DNA kit, transcriptomic libraries with the NEBNext Ultra II RNA kit (both New England Biolabs), and sequencing was carried out on an Illumina NovaSeq X platform using 25B flow cells in a 2 × 151 bp configuration.

Metagenome-assembled-genomes (MAGs)

For assembly of the MAGs from the four metagenome samples, the strategies previously established for creating rumen and human microbiome MAGs were applied[76,77]. The approach involved reconstructing bacterial contigs/scaffolds from metagenomic reads, binning them, grouping based on species-level inter-sample genomes, and finally generating non-redundant assemblies. Initially, metagenome assembly was applied separately to each sample using metaSPAdes from SPAdes genome assembler v4.0.0[78]. A co-assembly was then produced by pooling all reads with MEGAHIT v1.2.9[79]. Each single-sample assembly and co-assembly was subsequently subjected to metagenomic binning, utilizing tetranucleotide frequency and contig abundance with MetaBAT2 v2.17[80]. This process generated a total of 83 bins, which were aggregated and dereplicated using dRep v3.5[81]. For dereplication, the default options were applied to ensure bins retained both completeness ≥75% and contamination ≤25%, as assessed by CheckM v1.2.3[82]. This process yielded five dereplicated MAGs. However, further inspection of the dereplication results revealed that while the bins were complete, they exhibited high strain heterogeneity and contamination, as indicated by the presence of multiple copies of marker genes, suggesting significant diversity among the assemblies within a given taxonomy (Fig. S2). Consequently, all 83 bins and unbinned contigs (hereafter referred to as MAGs) were retained for further gene annotation and abundance estimation.

Taxonomic classification and gene prediction

The taxonomic classification of all bins was conducted using GTDB-Tk v2.4.0[83]. Among these, 16 MAGs were identified at the species level (7 species occurring in individual sample bins as well as co-assembly bins) and 40 MAG bins were categorized as undefined Bacteria/Archaea or remained completely unclassified. Classifying genomes assigned to uncharacterized phyla or lineages can be challenging, as these may not be well-represented in the GTDB-Tk's reference tree[83]. GTDB-Tk may struggle to accurately classify genomes with mosaic structures (regions from different lineages), especially if those regions have high sequence similarity to other parts of the genome, as we see in this study with multiple single-copy marker genes predicted by GTDB-Tk and CheckM[84](Data S2). While research suggests that contamination has a limited impact on GTDB-Tk classifications, it's still a potential concern, particularly with metagenome-assembled genomes (MAGs)[84]. The bin classified as family *Beggiatoaceae* and genus *UBA10656* was co-assembled from all the metagenome samples, indicating lower abundance in individual samples and a mosaic genome that is 44.8% complete, 2.3% contamination and 5.9% strain heterogeneity based on the presence of single-copy genes predicted by CheckM.

Unclassified MAG bins, constraints to avoid false positives by binning tool, leading to unbinned contigs that have lower coverage or smaller contig lengths to get a good representation of the organism's signature. But these unbinned contigs did capture marker genes for Archaea and Bacteria as predicted by GTDB-tk (Data S1). There have been very prominent representations of "unclassified Archaea" or "unclassified Bacteria" in each individual season with high abundance in the respective season (Fig. S3). But not necessarily all the unbinned contigs belong to Archaea or Bacteria, prompting further analysis with the deep-learning tool tiara v1.0.3[85] to identify eukaryotic sequences within the metagenomic datasets (Fig. S4D). Based on Tiara's categorization of contigs/scaffolds, gene annotation was carried out using Prokka v1.14.6[86]. Genes were predicted for contigs/scaffolds classified as Archaea, Bacteria, mitochondrion, prokaryote, and unknown. Prokka v1.14.6 provided gene sequence predictions, gene names, enzyme numbers, COG, and product descriptions. The quality-controlled sequence reads (post-adapter removal) were mapped to MAGs and genes, including eukaryotic and plastid contigs/scaffolds, using salmon v1.10.3[87,88]. Data S2 and Fig. S4A–C provide an overview of the mapping percentages for each sample.

Abundances of different taxonomies among the metagenome and metatranscriptome samples

Since the metagenome samples had no replicates, differential analysis was not possible. After mapping the reads to MAGs, the MAGs with identical taxonomy as defined by GTDB-tk were aggregated together. The difference among the four time points is shown using read-normalizing metrics such as robust centered log-ratio (rCLR) and/or z-scores after normalizing for library sizes. rCLR normalizes the data by adjusting for the compositional nature of metagenomic counts, making it a ratio-based transformation. The rCLR transformation allows you to interpret the values in terms of log-ratios (relative differences in species abundances compared to the geometric mean). Z-score Transformation normalizes the data by centering and scaling to unit variance.

Differential analysis of the genes and predicting enriched pathways

Quality control of gene abundances was conducted between the metagenome and metatranscriptome after normalizing raw counts to library size using Counts per Million (CPM). Genes with low counts across samples were removed. A noticeable trend was observed with rRNA and tmRNA: as the metagenome gene "copy number" increases, there is a corresponding increase in metatranscriptome expression, though this is not consistent in all cases (Fig. S2B). However, this trend is not seen in protein-coding genes (CDS) due to insufficient coverage, likely caused by the lack of rRNA depletion before sequencing. For subsequent differential expression and pathway analyses, only CDSs were considered.

Differential gene expression analysis and enriched pathway analysis was carried out using the Bioconductor package limma v3.60.6[89] and its function FRY[90], respectively. Prokka's predicted enzyme numbers were used to assign KEGG modules to carry out gene-set enrichment analysis using limma's FRY. FRY (Fry's Rotation Gene Set Test) is a method for identifying differential expression across gene sets using linear models. FRY tests whether groups of genes are collectively up- or down-regulated, without needing extensive rotations or simulations. FRY's output includes *p*-values for directional and mixed (non-directional) expression changes across gene sets, with False Discovery Rate adjustments for multiple testing. Caveats related to the metagenomic and metatranscriptomic data are summarized in Text S5.

Data availability

The 16S rRNA raw data generated in this study was deposited at the Sequence Read Archive under submission number SUB15462519 of NCBI (National Center for Biotechnology Information) under the BioProject ID PRJNA1288741 and BioSample accessions SAMN49948525 - SAMN49948656. Metagenome and metatranscriptomic data were deposited into the NCBI's SRA database as well under the BioProject ID PRJNA1286155, BioSample accessions SAMN49793412 - SAMN49793427 and are available at the following URL: https://www.ncbi.nlm.nih.gov/bioproject/PRJNA1286155. The bash and R-scripts written while analysing the metagenome and metranscriptome data is available on Github https://github.com/shubavarshini/marine_metagenome_metatranscriptome/wiki. The geochemical data from Boknis Eck is available from PANGAEA, https://doi.org/10.1594/PANGAEA.973020, https://doi.pangaea.de/10.1594/PANGAEA.976764, https://doi.org/10.1594/PANGAEA.974076, https://doi.pangaea.de/10.1594/PANGAEA.987156.

Received: 18 March 2026; Accepted: 22 September 2026;
Published online: 23 October 2026

References

1. Schmidtko, S., Stramma, L. & Visbeck, M. Decline in global oceanic oxygen content during the past five decades. *Nature* **542**, 335–339 https://doi.org/10.1038/nature21399 (2017).
2. Breitburg, D. et al. Declining oxygen in the global ocean and coastal waters. *Science* **359**, eaam7240 https://doi.org/10.1126/science.aam7240 (2018).
3. Brauko, K. M. et al. Marine heatwaves, sewage and eutrophication combine to trigger deoxygenation and biodiversity loss: a SW Atlantic Case Study. *Front. Mar. Sci.* **7**, 590258 https://doi.org/10.3389/fmars.2020.590258 (2020).
4. Carstensen, J., Andersen, J. H., Gustafsson, B. G. & Conley, D. J. Deoxygenation of the Baltic Sea during the last century. *Proc. Natl. Acad. Sci. USA* **111**, 5628–5633 https://doi.org/10.1073/pnas.1323156111 (2014).
5. Kabel, K. et al. Impact of climate change on the Baltic Sea ecosystem over the past 1,000 years. *Nat. Clim. Change* **2**, 871–874 https://doi.org/10.1038/nclimate1595 (2012).
6. Liblik, T. & Lips, U. Stratification has strengthened in the Baltic Sea – an analysis of 35 years of observational data. *Front. Earth Sci.* **7**, 174 https://doi.org/10.3389/feart.2019.00174 (2019).
7. Jutterström, S., Andersson, H. C., Omstedt, A. & Malmaeus, J. M. Multiple stressors threatening the future of the Baltic Sea–Kattegat marine ecosystem: Implications for policy and management actions. *Mar. Pollut. Bull.* **86**, 468–480 https://doi.org/10.1016/j.marpolbul.2014.06.027 (2014).
8. Meier, H. E. M., Väli, G., Naumann, M., Eilola, K. & Frauen, C. Recently accelerated oxygen consumption rates amplify deoxygenation in the Baltic Sea. *J. Geophys. Res. Oceans* **123**, 3227–3240 https://doi.org/10.1029/2017JC013686 (2018).
9. Reusch, T. B. H. et al. The Baltic Sea as a time machine for the future coastal ocean. *Sci. Adv.* **4**, eaar8195 https://doi.org/10.1126/sciadv.aar8195 (2018).
10. Hepach, H. et al. Enhanced warming and bacterial biomass production as key factors for coastal hypoxia in the southwestern Baltic Sea. *Sci. Rep.* **14**, 29442 https://doi.org/10.1038/s41598-024-80451-w (2024).
11. Wallmann, K. et al. Erosion of carbonate-bearing sedimentary rocks may close the alkalinity budget of the Baltic Sea and support atmospheric CO_2 uptake in coastal seas. *Front. Mar. Sci.* **9**,968069 https://doi.org/10.3389/fmars.2022.96 (2022).
12. Dale, A. W., Bertics, V. J., Treude, T., Sommer, S. & Wallmann, K. Modeling benthic-pelagic nutrient exchange processes and porewater distributions in a seasonally hypoxic sediment: evidence for massive phosphate release by *Beggiatoa*? *Biogeosciences* **10**, 629–651 https://doi.org/10.5194/bg-10-629-2013 (2013).
13. Hansen, H. P., Giesenhagen, H. C. & Behrends, G. Seasonal and long-term control of the bottom water oxygen deficiency in a stratified shallow water coastal system. *ICES J. Mar. Sci.* **56**, 65–71 (1999).
14. Graf, G., Schulz, R., Peinert, R. & Meyer-Reil, L. A. Benthic response to sedimentation events during autumn to spring at a shallow-water station in the Western Kiel Bight. *Mar. Biol.* **77**, 235–246 https://doi.org/10.1007/BF00395812 (1983).
15. Lennartz, S. T. et al. Long-term trends at the Boknis Eck time series station (Baltic Sea), 1957-2013: does climate change counteract the decline in eutrophication? *Biogeosciences* **11**, 6323–6339 https://doi.org/10.5194/bg-11-6323-2014 (2014).
16. Plass, A., Retschko, A.-K., Türk, M., Fischer, T. & Scholz, F. A novel device for trace metal-clean sampling of bottom water and suspended particles at the ocean's lower boundary: the Benthic Trace Profiler. *Limnol. Oceanogr.: Methods* **20**, 102–114 https://doi.org/10.1002/lom3.10473 (2022).
17. Philip A. et al. HELCOM thematic assessment of eutrophication 2016–2021. *Balt. Sea Environ. Proc.* **192**, https://helcom.fi/post_type_publ/holas3_eut/ (2023).
18. Perner, M. et al. Environmental changes affect the microbial release of hydrogen sulfide and methane from sediments at Boknis Eck (SW Baltic Sea). *Front. Microbiol.* **13**, 1096062 https://doi.org/10.3389/fmicb.2022.1096062 (2022).

19. Sinkko, H. et al. Increasing oxygen deficiency changes rare and moderately abundant bacterial communities in coastal soft sediments. *Sci. Rep.* **9**, 16341 https://doi.org/10.1038/s41598-019-51432-1 (2019).
20. Broman, E., Sjöstedt, J., Pinhassi, J. & Dopson, M. Shifts in coastal sediment oxygenation cause pronounced changes in microbial community composition and associated metabolism. *Microbiome* **5**, 96 https://doi.org/10.1186/s40168-017-0311-5 (2017).
21. Lipsewers, Y. et al. Impact of seasonal hypoxia on activity and community structure of Chemolithoautotrophic bacteria in a coastal sediment. *Appl. Environ. Microbiol.* **83**, e03517–03516 https://doi.org/10.1128/AEM.03517-16 (2017).
22. Jørgensen, B. B. Mineralization of organic matter in the sea bed—the role of sulphate reduction. *Nature* **296**, 643–645 https://doi.org/10.1038/296643a0 (1982).
23. Middelburg, J. J. & Levin, L. A. Coastal hypoxia and sediment biogeochemistry. *Biogeosciences* **6**, 1273–1293 https://doi.org/10.5194/bg-6-1273-2009 (2009).
24. Bertics, V. J. et al. Occurrence of benthic microbial nitrogen fixation coupled to sulfate reduction in the seasonally hypoxic Eckernförde Bay, Baltic Sea. *Biogeosciences* **10**, 1243–1258 https://doi.org/10.5194/bg-10-1243-2013 (2013).
25. Treude, T., Krüger, M., Boetius, A. & Jørgensen, B. B. Environmental control on anaerobic oxidation of methane in the gassy sediments of Eckernförde Bay (German Baltic). *Limnol. Oceanogr.* **50**, 1771–1786 https://doi.org/10.4319/lo.2005.50.6.1771 (2005).
26. Yao, C., Zhang, Q., Lin, X., Zhao, J. & Zhang, X. Seasonal hypoxia enhances benthic nitrogen fixation and shapes specific diazotrophic community in the eutrophic Marine Ranch. *Processes.***11**, 138 http://doi.org/10.3390/pr11010138 (2023)
27. van de Velde, S. J., Reinhard, C. T., Ridgwell, A. & Meysman, F. J. R. Bistability in the redox chemistry of sediments and oceans. *Proc. Natl. Acad. Sci. USA* **117**, 33043–33050 https://doi.org/10.1073/pnas.2008235117 (2020).
28. Seitaj, D. et al. Cable bacteria generate a firewall against euxinia in seasonally hypoxic basins. *Proc. Natl. Acad. Sci. USA* **112**, 13278–13283 https://doi.org/10.1073/pnas.1510152112 (2015).
29. Fennel, K. & Testa, J. M. Biogeochemical controls on coastal hypoxia. *Annu. Rev. Mar. Sci.* **11**, 105–130 https://doi.org/10.1146/annurev-marine-010318-095138 (2019).
30. Wu D. Lim E. Vaillant F. Asselin-Labat M.-L. Visvader J.E. & Smyth G.K. ROAST: rotation gene set tests for complex microarray experiments. *Bioinformatics* **26**, 2176–2182 https://doi.org/10.1093/bioinformatics/btq401 (2010).
31. Kanehisa M. Furumichi M. Sato Y. Matsuura Y. & Ishiguro-Watanabe M. KEGG: biological systems database as a model of the real world. *Nucleic Acids Res.* **53**, D672–D677 (2025) https://doi.org/10.1093/nar/gkae909.
32. Wardman, J. F. & Withers, S. G. Carbohydrate-active enzyme (CAZyme) discovery and engineering via (Ultra)high-throughput screening. *RSC Chem. Biol.* **5**, 595–616 https://doi.org/10.1039/D4CB00024B (2024).
33. Teske, A. & Salman, V. The family *Beggiatoaceae*. in *The Prokaryotes: Gammaproteobacteria* (eds Rosenberg E., DeLong E. F., Lory S., Stackebrandt E. & Thompson F.) https://doi.org/10.1007/978-3-642-38922-1_290 (Springer, Berlin, Heidelberg, 2014).
34. Middelburg, J. J., Vlug, T. & van der Nat, F. J. W. A. Organic matter mineralization in marine systems. *Glob. Planet Change* **8**, 47–58 https://doi.org/10.1016/0921-8181(93)90062-S (1993).
35. Xie, N. et al. NAD+ metabolism: pathophysiologic mechanisms and therapeutic potential. *Signal Transduct. Target. Ther.* **5**, 227 https://doi.org/10.1038/s41392-020-00311-7 (2020).
36. Kappler, A. et al. An evolving view on biogeochemical cycling of iron. *Nat. Rev. Microbiol.* **19**, 360–374 https://doi.org/10.1038/s41579-020-00502-7 (2021).
37. Schoonen, M. A. A. Mechanisms of sedimentary pyrite formation. in *Sulfur Biogeochemistry - Past and Present* (eds Amend J. P., Edwards K. J. & Lyons T. W.) https://doi.org/10.1130/0-8137-2379-5.117 (Geological Society of America, 2004).
38. Postma, D. Pyrite and siderite formation in brackish and freshwater swamp sediments. *Am. J. Sci.* **282**, 1151–1183 (1982).
39. Dahl, C. et al. Structural and molecular genetic insight into a widespread sulfur oxidation pathway. *J. Mol. Biol.* **384**, 1287–1300 https://doi.org/10.1016/j.jmb.2008.10.016 (2008).
40. Hoffmann, K. et al. Diversity and metabolism of Woeseiales bacteria, global members of marine sediment communities. *ISME J.* **14**, 1042–1056 https://doi.org/10.1038/s41396-020-0588-4 (2020).
41. Leang, C., Qian, X., Mester, T. & Lovley Derek, R. Alignment of the c-type cytochrome OmcS along Pili of Geobacter sulfurreducens. *Appl. Environ. Microbiol.* **76**, 4080–4084 https://doi.org/10.1128/AEM.00023-10 (2010).
42. Adam-Beyer, N., Deusner, C., Schmidt, M. & Perner, M. Microbial hydrogen oxidation potential in seasonally hypoxic Baltic Sea sediments. *Front. Microbiol.* **16,**1565157 https://doi.org/10.3389/fmicb.2025.1565157 (2025).
43. Maltby, J. et al. Microbial methanogenesis in the sulfate-reducing zone of sediments in the Eckernforde Bay, SW Baltic Sea. *Biogeosciences* **15**, 137–157 https://doi.org/10.5194/bg-15-137-2018 (2018).
44. Kato, N., Yurimoto, H. & Thauer, R. K. The physiological role of the ribulose monophosphate pathway in bacteria and archaea. *Biosci. Biotechnol. Biochem.* **70**, 10–21 https://doi.org/10.1271/bbb.70.10 (2006).
45. Wu, T. et al. Engineering a synthetic energy-efficient formaldehyde assimilation cycle in Escherichia coli. *Nat. Commun.* **14**, 8490 https://doi.org/10.1038/s41467-023-44247-2 (2023).
46. Klimek, D., Herold, M. & Calusinska, M. Comparative genomic analysis of Planctomycetota potential for polysaccharide degradation identifies biotechnologically relevant microbes. *BMC Genomics* **25**, 523 https://doi.org/10.1186/s12864-024-10413-z (2024).
47. Klimek, D. et al. Insights into the phylogenetic and metabolic diversity of Planctomycetota in anaerobic digesters and the isolation of novel Thermoguttaceae species. *FEMS Microbiol. Ecol.* **101**, fiaf025 https://doi.org/10.1093/femsec/fiaf025 (2025).
48. Wegner, C.-E. et al. Expression of sulfatases in Rhodopirellula baltica and the diversity of sulfatases in the genus Rhodopirellula. *Mar. Genomics* **9**, 51–61 https://doi.org/10.1016/j.margen.2012.12.001 (2013).
49. Momper, L., Aronson, H. S. & Amend, J. P. Genomic description of '*Candidatus* Abyssubacteria,' a novel subsurface lineage within the candidate Phylum Hydrogenedentes. *Front. Microbiol.* **9**, 1993 https://doi.org/10.3389/fmicb.2018.01993 (2018).
50. Vitorino, I. R. & Lage, O. M. The Planctomycetia: an overview of the currently largest class within the phylum Planctomycetes. *Antonie van. Leeuwenhoek* **115**, 169–201 https://doi.org/10.1007/s10482-021-01699-0 (2022).
51. Gade, D., Stührmann, T., Reinhardt, R. & Rabus, R. Growth phase dependent regulation of protein composition in *Rhodopirellula baltica*. *Environ. Microbiol.* **7**, 1074–1084 https://doi.org/10.1111/j.1462-2920.2005.00784.x (2005).
52. Kadnikov, V. V. et al. Phylogeny and physiology of candidate phylum BRC1 inferred from the first complete metagenome-assembled genome obtained from deep subsurface aquifer. *Syst. Appl. Microbiol.* **42**, 67–76 https://doi.org/10.1016/j.syapm.2018.08.013 (2019).
53. Suominen, S. et al. Organic matter type defines the composition of active microbial communities originating from anoxic Baltic Sea sediments. *Front. Microbiol.* **12,** 628301 https://doi.org/10.3389/fmicb.2021.628301 (2021).

54. Elshahed, M. et al. Phylogenetic and metabolic diversity of *Planctomycetes* from anaerobic, sulfide- and sulfur-rich Zodletone Spring, Oklahoma. *Appl. Environ. Microbiol.* **73**, 4707–4716 http://doi.org/10.1128/AEM.00591-07 (2007).
55. Mußmann, M. et al. Phylogeny and distribution of nitrate-storing Beggiatoa spp. in coastal marine sediments. *Environ. Microbiol.* **5**, 523–533 https://doi.org/10.1046/j.1462-2920.2003.00440.x (2003).
56. Hedges, J. I. et al. Sedimentary organic matter preservation; a test for selective degradation under oxic conditions. *Am. J. Sci.* **299**, 529–555 https://doi.org/10.2475/ajs.299.7-9.529 (1999).
57. Adam, N. et al. Deltaproteobacterium Strain KaireiS1, a mesophilic, hydrogen-oxidizing and sulfate-reducing bacterium from an inactive deep-sea hydrothermal chimney. *Front. Microbiol.* **12**, 686276. https://doi.org/10.3389/fmicb.2021.686276 (2021).
58. Wagner, T., Watanabe, T. & Shima, S. Hydrogenotrophic Methanogenesis. in *Biogenesis of Hydrocarbons* (eds Stams A. J. M. & Sousa D.) 385–397 (Springer International Publishing, 2018).
59. Zhao, L. et al. Effect of marine anoxia on the conversion of macroalgal biomass to refractory dissolved organic carbon. *Mar. Environ. Res.* **204**, 106956 https://doi.org/10.1016/j.marenvres.2025.106956 (2025).
60. Robador, A. et al. Activity and community structures of sulfate-reducing microorganisms in polar, temperate and tropical marine sediments. *ISME J.* **10**, 796–809 https://doi.org/10.1038/ismej.2015.157 (2016).
61. Sagemann, J., Jørgensen, B. B. & Greeff, O. Temperature dependence and rates of sulfate reduction in cold sediments of Svalbard, Arctic Ocean. *Geomicrobiol. J.* **15**, 85–100 https://doi.org/10.1080/01490459809378067 (1998).
62. Zhou, C. et al. Phosphorus mobilization in sulfidic sediments in the Baltic Sea. *Sci. Total Environ.* **907**, 168000 https://doi.org/10.1016/j.scitotenv.2023.168000 (2024).
63. Lehtimäki, M., Sinkko, H. & Tallberg, P. The role of oxygen conditions in the microbial dissolution of biogenic silica under brackish conditions. *Biogeochemistry* **129**, 355–371 http://doi.org/10.1007/s10533-016-0237-1 (2016).
64. Vázquez-Domínguez, E., Gasol, J. M. & Vaque, D. Temperature effects on the heterotrophic bacteria, heterotrophic nanoflagellates, and microbial top predators of the NW Mediterranean. *Aquat. Microb. Ecol.* **67**, 107–121 http://doi.org/10.3354/ame01583 (2012).
65. Meyer, B. & Kuever, J. Molecular analysis of the diversity of sulfate-reducing and sulfur-oxidizing prokaryotes in the environment, using aprA as functional marker gene. *Appl. Environ. Microbiol.* **73**, 7664–7679 https://doi.org/10.1128/AEM.01272-07 (2007).
66. Lloyd, K. et al. Phylogenetically novel uncultured microbial cells dominate earth microbiomes. *mSystems* **3,** 10.1128/mysystems.00055-00018 https://doi.org/10.1128/msystems.00055-18 (2018).
67. Herszage, J. & dos Santos Afonso, M. Mechanism of hydrogen sulfide oxidation by manganese(IV) oxide in aqueous solutions. *Langmuir* **19**, 9684–9692 https://doi.org/10.1021/la034016p (2003).
68. Chandel, N. S. Nucleotide metabolism. *Cold Spring Harbor Perspect. Biol.* **13,** a040592 https://doi.org/10.1101/cshperspect.a040592 (2021).
69. Dailey Harry, A. et al. Prokaryotic heme biosynthesis: multiple pathways to a common essential product. *Microbiol. Mol. Biol. Rev.* **81** https://doi.org/10.1128/mmbr.00048-16 (2017).
70. Begley, T. P., Kinsland, C., Mehl, R. A., Osterman, A. & Dorrestein, P. The biosynthesis of nicotinamide adenine dinucleotides in bacteria. in *Vitamins & Hormones* **61**, 103–119 http://doi.org/10.1016/S0083-6729(01)61003-3 (Academic Press, 2001).
71. Dale, A. W., Treude, T., Bleyer, A. & Domeyer, B. *Porewater geochemistry at Eckernförde Bay (Boknis Eck) from 2010 to 2011* (PANGAEA, 2012) https://doi.org/10.1594/PANGAEA.778723).
72. Berner, R. A. Sedimentary pyrite formation: an update. *Geochim. Cosmochim. Acta* **48**, 605–615 https://doi.org/10.1016/0016-7037(84)90089-9 (1984).
73. Collins, P. C., Carlsson, J., Rowcroft, P. & Tibbles, B. Ecosystem status of the deep Black Sea, soft sediment, benthic community. *Mar. Policy* **73**, 216–223 https://doi.org/10.1016/j.marpol.2016.07.016 (2016).
74. Piker, L., Schmaljohann, R. & Imhoff, J. F. Dissimilatory sulfate reduction and methane production in Gotland Deep sediments (Baltic Sea) during a transition period from oxic to anoxic bottom water (1993-1996). *Aquat. Microb. Ecol.* **14**, 183–193 https://doi.org/10.3354/ame014183 (1998).
75. Røy, H., Weber, H. S., Tarpgaard, I. H., Ferdelman, T. G. & Jørgensen, B. B. Determination of dissimilatory sulfate reduction rates in marine sediment via radioactive 35S tracer. *Limnol. Oceanogr. Methods* **12**, 196–211 https://doi.org/10.4319/lom.2014.12.196 (2014).
76. Pasolli, E. et al. Extensive unexplored human microbiome diversity revealed by over 150,000 genomes from metagenomes spanning age, geography, and lifestyle. *Cell* **176**, 649–662.e620 https://doi.org/10.1016/j.cell.2019.01.001 (2019).
77. Stewart, R. D. et al. Assembly of 913 microbial genomes from metagenomic sequencing of the cow rumen. *Nat. Commun.* **9**, 870 https://doi.org/10.1038/s41467-018-03317-6 (2018).
78. Nurk, S., Meleshko, D., Korobeynikov, A. & Pevzner, P. A. metaSPAdes: a new versatile metagenomic assembler. *Genome Res.* **27**, 824–834 https://doi.org/10.1101/gr.213959.116 (2017).
79. Li, D., Liu, C.-M., Luo, R., Sadakane, K. & Lam, T.-W. MEGAHIT: an ultra-fast single-node solution for large and complex metagenomics assembly via succinct de Bruijn graph. *Bioinformatics* **31**, 1674–1676 https://doi.org/10.1093/bioinformatics/btv033 (2015).
80. Kang, D. D. et al. MetaBAT 2: an adaptive binning algorithm for robust and efficient genome reconstruction from metagenome assemblies. *PeerJ* **7**, e7359 https://doi.org/10.7717/peerj.7359 (2019).
81. Olm, M. R., Brown, C. T., Brooks, B. & Banfield, J. F. dRep: a tool for fast and accurate genomic comparisons that enables improved genome recovery from metagenomes through de-replication. *ISME J.* **11**, 2864–2868 https://doi.org/10.1038/ismej.2017.126 (2017).
82. Parks, D. H., Imelfort, M., Skennerton, C. T., Hugenholtz, P. & Tyson, G. W. CheckM: assessing the quality of microbial genomes recovered from isolates, single cells, and metagenomes. *Genome Res.* **25**, 1043–1055 https://doi.org/10.1101/gr.186072.114 (2015).
83. Chaumeil, P.-A., Mussig, A. J., Hugenholtz, P. & Parks, D. H. GTDB-Tk: a toolkit to classify genomes with the Genome Taxonomy Database. *Bioinformatics* **36**, 1925–1927 https://doi.org/10.1093/bioinformatics/btz848 (2020).
84. Mussig, A. J. et al. Putative genome contamination has minimal impact on the GTDB taxonomy. *Microbial. Genom.* **10**, 001256 https://doi.org/10.1099/mgen.0.001256 (2024).
85. Karlicki, M., Antonowicz, S. & Karnkowska, A. Tiara: deep learning-based classification system for eukaryotic sequences. *Bioinformatics* **38**, 344–350 https://doi.org/10.1093/bioinformatics/btab672 (2022).
86. Seemann, T. Prokka: rapid prokaryotic genome annotation. *Bioinformatics* **30**, 2068–2069 https://doi.org/10.1093/bioinformatics/btu153 (2014).
87. Patro, R., Duggal, G., Love, M. I., Irizarry, R. A. & Kingsford, C. Salmon provides fast and bias-aware quantification of transcript expression. *Nat. Methods* **14**, 417–419 https://doi.org/10.1038/nmeth.4197 (2017).
88. Srivastava, A. et al. Alignment and mapping methodology influence transcript abundance estimation. *Genome Biol.* **21**, 239 https://doi.org/10.1186/s13059-020-02151-8 (2020).
89. Ritchie, M. E. et al. limma powers differential expression analyses for RNA-sequencing and microarray studies. *Nucleic Acids Res.* **43**, e47–e47 https://doi.org/10.1093/nar/gkv007 (2015).

90. Wu, D. et al. ROAST: rotation gene set tests for complex microarray experiments. *Bioinformatics* **26**, 2176–2182 https://doi.org/10.1093/bioinformatics/btq401 (2010).
91. Bange, H. W. & Malien, F. Hydrochemistry from time series station Boknis Eck from 1957 to 2014. *PANGAEA* https://doi.org/10.1594/PANGAEA.855693 (2015).

Acknowledgements

We thank the captain and crew of the FK Littorina for helping to obtain the samples. Elisabeth Kirst, Jeannine Wilde, Tatiana Borodina and Janine Altmüller from the BIH/MDC Genomics Technology Platform are acknowledged for metagenome/transcriptome sequencing. We thank Prof. Dr. rer. nat. Dieter Beule, Head of Core Unit Bioinformatics and HPC Unit in BIH@Charité, Berlin, for providing the computational resources necessary for metagenome and metatranscriptome data analysis. We also thank Ronny Baaske, Gabriele Schüßler, Bettina Domeyer, Regina Surberg, and Anke Bleyer for laboratory analytics of sediment samples from Boknis Eck. We thank Kastriot Qelaj, Kerstin Nachtigall and Levka Hansen for the monthly nutrient, chl a and O_2 water column measurements from Boknis Eck.

Author contributions

S.V.A.**:** Formal analysis, Data curation, Validation, Visualization, Writing – Review & Editing. S.B.B.**:** Investigation, Data curation, Validation, Formal analysis, Visualization, Writing – Review & Editing. N.A.B.: Investigation, Data curation, Writing – Review & Editing. K.L.M.: Investigation, Supervision, Writing – Review & Editing. K.W.**:** Methodology, Formal analysis, Validation, Writing – Review & Editing. H.W.B.: Investigation, Data curation. H.H.: Investigation, Data curation. M.T.: Data curation, J.F.: Methodology, E.W.**:** Investigation, Resources. M.L.**:** Investigation, Resources. I.D.**:** Investigation. F.S.: Writing – Review & Editing. M.P.: Conceptualization, Investigation, Data curation, Validation, Project administration, Supervision, Funding acquisition, Writing – Original Draft.

Funding

This study was funded within the framework of the “program-oriented funding” (PoF IV, Topic 6) of the Helmholtz Association and by the Federal Ministry of Research, Technology and Space (BMFTR) (Project PrimePrevention, awarded to MP Grant No. 03F0953C) in the framework of the Deutsche Allianz für Meeresforschung (DAM) mission mareXtreme. This work was further supported by the DFG Research Infrastructure NGS_CC (project 407495230) as part of the Next Generation Sequencing Competence Network (project 423957469). Open Access funding enabled and organized by Projekt DEAL.

Competing interests

The authors declare no competing interests.

Additional information

Supplementary information The online version contains supplementary material available at https://doi.org/10.1038/s43247-026-04120-8.

Correspondence and requests for materials should be addressed to Mirjam Perner.

Peer review information *Communications Earth & Environment* thanks all reviewer(s) for their contribution to the peer review of this work. Primary Handling Editors: Erika Buscardo and Marisa McDonald. A peer review file is available.

Reprints and permissions information is available at http://www.nature.com/reprints

Publisher’s note Springer Nature remains neutral with regard to jurisdictional claims in published maps and institutional affiliations.

Open Access This article is licensed under a Creative Commons Attribution 4.0 International License, which permits use, sharing, adaptation, distribution and reproduction in any medium or format, as long as you give appropriate credit to the original author(s) and the source, provide a link to the Creative Commons licence, and indicate if changes were made. The images or other third party material in this article are included in the article's Creative Commons licence, unless indicated otherwise in a credit line to the material. If material is not included in the article's Creative Commons licence and your intended use is not permitted by statutory regulation or exceeds the permitted use, you will need to obtain permission directly from the copyright holder. To view a copy of this licence, visit http://creativecommons.org/licenses/by/4.0/.

© The Author(s) 2026